ORGANIZATION FOR NUCLEAR RESEARCH

CERN-PRE-78-154

A MODEL-INDEPENDENT PARTIAL WAVE ANALYSIS OF THE $\pi^+\pi^-$ SYSTEM PRODUCED AT LOW FOUR-MOMENTUM TRANSFER IN THE REACTION $\pi^- p\uparrow \to \pi^+\pi^- n$ AT 17.2 GeV/c

(CERN-Cracow-Munich Collaboration)

H. Becker*), G. Blanar, W. Blum, M. Cerrada, H. Dietl, J. Gallivan, B. Gottschalk**), G. Grayer***), G. Hentschel†), E. Lorenz, G. Lütjens, G. Lutz, W. Männer, D. Notz††), R. Richter, U. Stierlin and B. Stringfellow×)

Max Planck Institute, Munich, Germany

V. Chabaud, B. Hyams and T. Papadopoulou××)

CERN, Geneva, Switzerland

J. de Groot×××)

Zeeman Laboratory, Amsterdam, The Netherlands

L. Görlich, B. Niczyporuk, K. Rybicki and A. Zalewska

Institute of Nuclear Physics, Cracow, Poland

Geneva - 29 September 1978

(Submitted to Nuclear Physics B)

---

*) Now at Technische Fachhochschule, Saarbrücken, Germany.

**) Visitor from Northeastern University, Boston, Mass., USA.

***) Now at Rutherford Laboratory, Chilton, Didcot, Oxon., England.

†) Now at the University of Frankfurt, Germany.

††) Now at DESY, Hamburg, Germany.

×) Now at the Nuclear Research Centre, Strasbourg, France.

××) Now at the National Technical University, Athens, Greece.

×××) Now at CERN, Geneva, Switzerland.

ABSTRACT

The $\pi^+\pi^-$ partial waves are studied up to the F-wave in the mass region from 580 to 1780 MeV/c^2 at low four-momentum transfer. The study is based on a previous hydrogen target experiment and a more recent polarized target experiment. Using the results of both experiments for $0.01 \leq |t| \leq 0.20$ GeV$^2/c^2$, a partial wave analysis is performed in each mass bin (Δm = 40 MeV/c^2) independently. For the first time a model-independent analysis has been possible, which enables us to check the assumptions made in previous studies. In general we find a unique solution determining the exact intensity of each partial wave. The uniqueness of our solution is related to the Barrelet zeros being real in the mass region where their imaginary parts were supposed to produce ambiguities. We observe a non-π exchange contribution even in the helicity m = 0 amplitudes. This effect (A_1 exchange and/or s-channel absorption) is stronger than previously expected but tends to decrease with the increasing $\pi\pi$ mass. Apart from the leading resonances (ρ,f,g) we see interesting structures in the lower partial waves.

1. INTRODUCTION

An extensive analysis of the $\pi^+\pi^-$ partial waves above 1 GeV became possible with the high-statistics experiment ($\sim$ 300,000 events) of the CERN-Munich group [1] at 17.2 GeV/c on a hydrogen target (hereafter called experiment I). Several studies were performed in the low four-momentum transfer regions ($|t| < 0.15$ GeV^2/c^2), all based on the results of this experiment. In the absence of polarization data, some physical assumptions had to be introduced in order to provide the missing constraints; these were the following:

a) s-channel nucleon spin flip dominance in the unnatural spin-parity amplitudes;

b) phase coherence of the unnatural spin-parity exchange amplitudes with helicity m = 0 and m = 1;

c) identical vanishing of m $\geq$ 2 t-channel moments (this assumption is well supported by the experimental values of moments).

In most studies an additional assumption was made, namely

d) averaging over the t-bin is permitted. This means that instead of extrapolation to the π pole, the partial wave analysis is done in a large t-bin in the physical t region.

Only assumption (d) is maintained in the present work.

One of the first studies in the mass region covered in the present work was done by the CERN-Munich Group [2], yielding a solution from 600 MeV/c^2 to 1900 MeV/c^2 with a $\rho'(1600)$ in the P-wave.

In other papers [3] the CERN-Munich Group and, independently, Estabrooks and Martin [4] applied the method of Barrelet zeros [5] to investigate ambiguities in the partial waves. While differing in many details, both approaches [3,4] led to the same two solutions (A,B) below $\sim$ 1450 MeV/c^2 and four (A,B,C,D) above this mass. The main difference between these solutions is the resonance structure of the lower waves (S,P,D) above $\sim$ 1450 MeV/c^2.

Shimada [6] showed that the measurement of other charge states should remove some of these solutions. In fact the raw $\pi^0\pi^0$ mass spectra obtained by the CERN-IHEP-Karlsruhe-Pisa-Vienna Collaboration [7] at 40 GeV/c seem to disagree with the solutions C and D.

Froggatt and Petersen [8] imposed fixed-t dispersion relations on $\pi\pi$ partial waves. They arrived at only one solution, β, which is of the B type, i.e. with the $\rho'(1600)$ resonance in the P-wave.

Martin and Pennington [9] also imposed analyticity in the form of fixed-t and fixed-u dispersion relations. They arrived at two solutions: α (of the A type; without the ρ') and β. The main physical differences between these two solutions are:

α) highly inelastic S-wave above the $\varepsilon(1200)$ resonance, very little or no $\rho'(1600)$ in the P-wave, and a new object called $f^*(1550)$ in the D-wave;

β) elastic S-wave vanishing around 1600 MeV, the $\rho'(1600)$ in the P-wave, and no $f^*(1550)$ in the D-wave.

Martin and Pennington have found also a third solution:

β') essentially similar to β but with stronger S-wave around 1600 MeV and weaker but still prominent $\rho'(1600)$.

In the present work we use the results of experiment I and our polarized target experiment (hereafter called II). The latter yielded $\sim$ 1,200,000 events of the reaction $\pi^- p \to \pi^+\pi^- n$ on a butanol (C_4H_9OH) target. About one third of them correspond to collisions with free protons (the hydrogen nuclei) with the average polarization P = 68%. Therefore we do not use the polarization-independent angular distribution from experiment II since this corresponds mostly to the protons bound in the carbon or oxygen nuclei; we use instead the results of experiment I. On the other hand, only free protons contribute to the polarization-dependent angular distribution in experiment II. As we will see, the very presence of the polarization effect rules out the basic assumption (a) used in all the above-mentioned studies. Combining the results of both experiments, we can perform a model-independent

partial wave analysis avoiding any *a priori* assumption throughout the paper. (The cut-off in both the angular momentum ℓ_{max} and the helicity $m_{max} = 1$ which we will use in the analysis has been motivated by the absence of moments t_M^L, with $L > 2\ell_{max}$ and $M > 2m_{max}$.)

Preliminary results of experiment II were presented previously [10]. The $\rho(770)$ mass region has been investigated in detail in refs. 11 and 12, which also deal with the apparatus, acceptance corrections, and the determination of the cross-section. The mathematical formalism used for describing nucleon polarization effects in this reaction (amplitudes, moments, and detailed relations between them) are described elsewhere [13].

2. VARIABLES, MOMENTS, AND AMPLITUDES

At a given energy the reaction in question may be described by the following five variables:

$m_{\pi\pi}$: effective mass of the $\pi\pi$ system

t: four-momentum transfer to the nucleon

ψ: polarization angle (the angle between the normal to the reaction plane and the polarization direction)

θ,ϕ: decay angles of the π^- in the $\pi^+\pi^-$ rest system (here the Gottfried-Jackson system).

Owing to parity conservation, the angular distribution for the reaction on a transversely polarized target is of the general form

$$I(m_{\pi\pi},t,\theta,\phi,\psi) = \sum_{L,M} t_M^L(m_{\pi\pi},t)\ \mathrm{Re}\ Y_M^L(\cos\theta,\phi) + P_t \cos\psi \sum_{L,M} p_M^L(m_{\pi\pi},t)\ \mathrm{Re}\ Y_M^L(\cos\theta,\phi)$$

$$+ P_t \sin\psi \sum_{L,M} r_M^L(m_{\pi\pi},t)\ \mathrm{Im}\ Y_M^L(\cos\theta,\phi)\ ,$$

where

P_t is the polarization component perpendicular to the beam direction (the full proton polarization $P \approx 68\%$ in our case), and

$Y_M^L(\cos\theta,\phi)$ are the spherical harmonic functions.

The full set of moments

$$t_M^L = \varepsilon_M \langle \mathrm{Re}\, Y_M^L(\cos\theta,\phi)\rangle = \frac{\varepsilon_M}{2\pi}\int I(\theta,\phi,\psi)\ \mathrm{Re}\, Y_M^L(\cos\theta,\phi)\ d\cos\theta\, d\phi\, d\psi$$

$$p_M^L = 2\varepsilon_M \langle \mathrm{Re}\, Y_M^L(\cos\theta,\phi)\cos\psi\rangle = \frac{\varepsilon_M}{2\pi}\int I(\theta,\phi,\psi)\cos\psi\ \mathrm{Re}\, Y_M^L(\cos\theta,\phi)\, d\cos\theta\, d\phi\, d\psi$$

$$r_M^L = 4\langle \mathrm{Im}\, Y_M^L(\cos\theta,\phi)\sin\psi\rangle = \frac{2}{\pi}\int I(\theta,\phi,\psi)\sin\psi\ \mathrm{Im}\, Y_M^L(\cos\theta,\phi)\ d\cos\theta\, d\phi\, d\psi\ ,$$

$$(\varepsilon_{M=0} = 1,\ \varepsilon_{M\neq 0} = 2)$$

and their dependence on effective mass $m_{\pi\pi}$ and four-momentum transfer t represent the complete basis of our analysis.

As we have already mentioned, we use the t_M^L moments from experiment I on the hydrogen target ($\sim$ 300,000 events). The p_M^L and r_M^L moments come from the polarized free protons in experiment II. The errors on these moments correspond to what would be expected from 60,000 measured events on 100% polarized protons.

Figure 1 shows the mass dependence of all t-channel moments for $0.01\ \mathrm{GeV}^2/c^2 \leq |t| \leq 0.20\ \mathrm{GeV}^2/c^2$. The moments are normalized so that $t_0^0 = 1/\sqrt{4\pi}$.

Following ref. 1 we restrict the analysis to $m_{\pi\pi}$ above 580 MeV/c^2, the upper limit (1780 MeV/c^2) being due to the acceptance restrictions of experiment II. The lower limit of the four-momentum transfer $|t|$ (0.01 GeV$^2/c^2$) was chosen above the kinematic limit for the highest mass considered. The following features of the moments are seen in fig. 1.

i) The p_M^L moments are generally of the opposite sign to that of the corresponding t_M^L moments, and are of comparable magnitude. The ratio p_M^L/t_M^L tends to decrease with increasing mass. For the ratio p_0^0/t_0^0, which is the left-right asymmetry, we find the values 0.5 (0.35) for the ρ (f) resonance on a scale

where the maximum value is 1. Between 1450 MeV/c^2 and 1600 MeV/c^2, rapid changes in the p_M^L moments occur. This effect is somewhat marginal statistically but follows the same pattern in the main moments (L = 2ℓ, M = 0). Above 1600 MeV/c^2 the p_M^L moments are consistent with zero within large errors.

ii) The r_M^L moments are compatible with zero over the whole mass range.

iii) All M ≥ 2 moments are negligible (M = 2 moments become large at high t). This fact led us to neglect amplitudes with m > 1 in the analysis.

The moments are related to the nucleon transversity amplitudes (spin component perpendicular to the reaction plane) by the following formulae (they are given explicitly in refs. 11-13):

$$t_M^L = \sum_{j,k} c_{jk}^{LM} \, \mathrm{Re}\left(U_{g_j} U_{g_k}^* + U_{h_j} U_{h_k}^* + N_{g_j} N_{g_k}^* + N_{h_j} N_{h_k}^* \right)$$

$$p_M^L = \sum_{j,k} c_{jk}^{LM} \, \mathrm{Re}\left(U_{g_j} U_{g_k}^* - U_{h_j} U_{h_k}^* - N_{g_j} N_{g_k}^* + N_{h_j} N_{h_k}^* \right)$$

$$r_M^L = \sum_{j,k} c_{jk}^{LM} \, \mathrm{Re}\left(-U_{g_j} N_{g_k}^* + U_{h_j} N_{h_k}^* + N_{g_j} U_{g_k}^* - N_{h_j} U_{h_k}^* \right)$$

where

U(N) denotes the unnatural (natural) spin parity exchange;

j or k stands for the dipion spin ℓ and helicity m indices;

c_{jk}^{LM} contains the Clebsch-Gordan coefficients and factors such as $\sqrt{2L+1}$.

Inspection of the structure of the formulae shows that there are no interference terms between the g and h amplitudes; therefore the phase between the sets of g and h amplitudes cannot be determined. However, we can determine everything (in principle) within each set of nucleon transversity amplitudes (hereafter referred to as transversity amplitudes) and this is why we use them in our analysis. Previous studies were always formulated in terms of helicity amplitudes. Their relations to transversity amplitudes are as follows:

$$\left.\begin{aligned} U_{g_m}^{\ell} &= \frac{1}{\sqrt{2}}\left(U_{n_m}^{\ell} + i\, U_{f_m}^{\ell}\right) \\ N_{g_m}^{\ell} &= \frac{1}{\sqrt{2}}\left(N_{n_m}^{\ell} - i\, N_{f_m}^{\ell}\right) \end{aligned}\right\} \text{recoil transversity down}$$

$$\left.\begin{aligned} U_{h_m}^{\ell} &= \frac{1}{\sqrt{2}}\left(U_{n_m}^{\ell} - i\, U_{f_m}^{\ell}\right) \\ N_{h_m}^{\ell} &= \frac{1}{\sqrt{2}}\left(N_{n_m}^{\ell} + i\, N_{f_m}^{\ell}\right) \end{aligned}\right\} \text{recoil transversity up}$$

In turn, the helicity amplitudes are defined as follows:

$$\left.\begin{aligned} U_{n_m}^{\ell} &= \frac{1}{\sqrt{2}}\left[\langle \ell,m,\tfrac{1}{2}|\tfrac{1}{2}\rangle + (-1)^m \langle \ell,-m,\tfrac{1}{2}|\tfrac{1}{2}\rangle\right] & U_{n_0}^{\ell} &= \langle \ell,0,\tfrac{1}{2}|\tfrac{1}{2}\rangle \\ N_{n_m}^{\ell} &= \frac{1}{\sqrt{2}}\left[\langle \ell,m,\tfrac{1}{2}|\tfrac{1}{2}\rangle - (-1)^m \langle \ell,-m,\tfrac{1}{2}|\tfrac{1}{2}\rangle\right] & N_{n_0}^{\ell} &\equiv 0 \end{aligned}\right\} \text{spin non-flip}$$

$$\left.\begin{aligned} U_{f_m}^{\ell} &= \frac{1}{\sqrt{2}}\left[\langle \ell,m,\tfrac{1}{2}|-\tfrac{1}{2}\rangle + (-1)^m \langle \ell,-m,\tfrac{1}{2}|-\tfrac{1}{2}\rangle\right] & U_{f_0}^{\ell} &= \langle \ell,0,\tfrac{1}{2}|-\tfrac{1}{2}\rangle \\ N_{f_m}^{\ell} &= \frac{1}{\sqrt{2}}\left[\langle \ell,m,\tfrac{1}{2}|-\tfrac{1}{2}\rangle - (-1)^m \langle \ell,-m,\tfrac{1}{2}|-\tfrac{1}{2}\rangle\right] & N_{f_0}^{\ell} &\equiv 0 \end{aligned}\right\} \text{spin flip .}$$

In the above formulae $\langle \ell,m,n|\lambda\rangle$ is the helicity amplitude describing the transition from the initial state with the target proton helicity $\lambda = \pm\frac{1}{2}$ to the final state with the recoil neutron helicity $n = \pm\frac{1}{2}$, and the dipion system characterized by the spin ℓ and helicity m.

Now let us express the physical assumption of π-exchange dominance in the reaction under consideration, in the language of both amplitudes. For the s-channel helicity amplitudes it is equivalent to spin-flip dominance, i.e. $U_{n_j} \equiv 0$ for any j, or for transversity amplitudes $U_{g_j} \equiv U_{h_j}$ for any j. Therefore any non-zero value of the p_M^L and r_M^L moments could come only from the natural exchange contribution, which is small at low four-momentum transfer. Thus the experimental p_M^L moments rule out assumption (a) of the introduction.

Before proceeding with the analysis, let us make a remark about the reference system. We use t-channel (Gottfried-Jackson system) moments. The relations between moments and amplitudes are valid for both s- and t-channel moments as long as the $\pi\pi$ helicities are chosen according to the given channel, and the nucleon helicities are defined in the s-channel. If we used the t-channel moments and t-channel helicities we would still obtain good results except for the phase between the natural and unnatural spin-parity exchange amplitudes. This could be corrected for by rotating this phase by the Wigner crossing angle (for its definition see ref. 13). The direction of this rotation depends on the sign of transversity. Since in any case we are not able to determine the relative phase between the natural and unnatural spin-parity exchange amplitudes (see below), this rotation does not make any difference in practice.

3. DETERMINATION OF THE TRANSVERSITY AMPLITUDES

We consider only amplitudes with $m \leq 1$. This is justified by the vanishing of the $M > 2$ t-channel moments and very small values of the $M = 2$ moments. This simplification, while important, is not essential for our analysis, since even with $m = 2$ amplitudes we have enough observables (considering $M > 2$ moments).

We divide the entire mass interval into three regions according to the highest wave that must be used (P, D, or F). The upper limits of the first two regions (900 MeV/c^2 and 1380 MeV/c^2) are justified *a posteriori* by the negligible intensity of the next wave (D or F). We could also check that there is sufficient consistency for the lower waves calculated with and without this wave. However, we have no evidence that the G-wave can be neglected at $\sim$ 1700 MeV/c^2 even though the $L \geq 7$ moments vanish within errors (see the relevant plots in ref. 1). On the contrary, Martin and Pennington [9] have shown a good case for the importance of this wave. Thus we are aware of the fact that our results may be somewhat distorted in the last few mass bins. Another reason for the possible distortion is the poor acceptance of experiment II at high mass.

The characteristics of each mass region are shown in table 1. When fitting the transversity amplitudes the following parameters are expected to be undetermined or ambiguous:

i) The over-all phase.

ii) The phase between the g and h amplitudes. The missing information could only be supplied by a measurement of the polarization of the recoil neutron. In the absence of this information we can determine everything inside each set of the transversity amplitudes and such quantities as $|g_m^j|^2 + |h_m^j|^2$, which is the intensity of each partial wave, or the ratio $|g_m^j|/|h_m^j|$. The deviation of this ratio from unity measures the lower limit of the spin non-flip amplitudes n_m^j. If $n_m^j = 0$ then $|g_m^j| = |h_m^j|$.

iii) The over-all sign of all relative phases inside each transversity set (g or h) can be changed.

iv) We expect also discrete ambiguities resulting from bilinear equations relating moments to amplitudes.

In practice the last item could be the most troublesome one. Therefore some effort was devoted to finding as many solutions as possible in each mass bin. It should be remembered that we perform an energy-independent analysis, and each mass bin is treated separately with many starting values for the fit. They are (see ref. 13 for details):

i) several sets of random values;

ii) exact analytical solutions of the equations relating moments to amplitudes -- this is possible only in the first mass region;

iii) analytical solutions assuming phase coherence as in the old studies -- this is done in the second and third mass regions;

iv) analytical solutions assuming that the P-wave is the weakest one (only in the second mass region).

The approximations in (iii) and (iv) are used only for determination of the starting values. It is always the exact formulae that we fit. This is done in 40 MeV/c^2 mass bins using the CERN MINUIT program [14]. The fit becomes more difficult and time-consuming as we include higher waves. Therefore we demand the MINOS error analysis (see ref. [14] for details) for all parameters only in the first mass region. In other mass regions these errors were requested only for the leading amplitudes (m = 0), the errors of other parameters being taken as the MIGRAD errors [14]. To facilitate the MINUIT task in the third mass region, we fixed the smallest amplitudes ($^{U}g_1^1$, $^{N}g_1^1$, $^{U}g_1^2$, $^{N}g_1^2$ and the relevant h amplitudes) at some reasonably small values. In most mass bins this condition could be partially or fully released once the proper solution had been found.

The fits are very good, as can be seen from the values of χ^2/d.f. in table 1. Apart from the mass regions 900-1100 MeV/c^2 and $\sim$ 1500 MeV/c^2, there is exactly one solution in each mass bin. (There is also some ambiguity at 1600 MeV/c^2 and 1680 MeV/c^2, but here the errors overlap. We select the solution with the lower χ^2.) The ambiguities in these mass regions may be due to relatively low statistics. Nevertheless even here one solution is usually favoured by demanding a resonance shape for the leading waves (P_0 and/or D_0 and/or F_0). The only ambiguity which we cannot resolve in our data is the S-wave ambiguity resembling the old "up-down" one. We will come back to the problem of ambiguities in section 6 when discussing the Barrelet zeros.

The phases between the natural and unnatural spin-parity exchange amplitudes cannot be reliably determined in the four-momentum transfer region under investigation. This is connected with the small values of the natural exchange amplitudes and vanishing of the r_M^L moments.

4. INTENSITIES OF THE PARTIAL WAVES

As we have already mentioned, the exact amount of each wave characterized by the dipion spin ℓ and helicity m can be determined as

$$|L_m|^2 = |g_m^\ell|^2 + |h_m^\ell|^2 = |n_m^\ell|^2 + |f_m^\ell|^2 \ .$$

Thus for the first time we can separate the individual partial waves. The partial-wave intensities thus obtained can be directly compared with the previous results without any complications due to the relations between helicity and transversity amplitudes.

The partial-wave cross-sections are shown in fig. 2. Each point represents the absolute intensity (in microbarns) of the given partial wave in a 40 MeV/c^2 mass bin and 0.01 GeV^2/c^2 $\leq |t| \leq$ 0.20 GeV^2/c^2 (we do not divide by the bin size). Thus

$$|S|^2 \propto \left(|{}^{U}g_0^0|^2 + |{}^{U}h_0^0|^2\right)$$

$$|P_0|^2 \propto \left(|{}^{U}g_0^1|^2 + |{}^{U}h_0^1|^2\right)$$

$$|P_U|^2 \propto \left(|{}^{U}g_1^1|^2 + |{}^{U}h_1^1|^2\right)$$

$$|P_N|^2 \propto \left(|{}^{N}g_1^1|^2 + |{}^{N}h_1^1|^2\right), \text{ etc.}$$

If there is more than one solution the full circle shows the solution which is more consistent with the tails of the leading resonances $\rho(770)$, $f(1270)$ and $g(1690)$ which dominate the P_0-, D_0- and F_0-waves, respectively. The choice is quite obvious around 1000 MeV/c^2 and less so around 1500 MeV/c^2. In the S-wave above the $\rho(770)$ resonance the full circles represent the solution that is more similar to the "down" solution generally favoured in previous studies.

We fit the intensities of the leading partial waves by the Breit-Wigner formula:

$$\frac{d^2\sigma}{dt\,dm_{\pi\pi}}\,|L_m|^2 = A\,\frac{m_{\pi\pi}^2}{q}\left|\frac{\sqrt{2J+1}\;m_R X_R \Gamma}{m_R^2 - m_{\pi\pi}^2 - i\,m_R\Gamma}\right|^2 ,$$

where

A = the normalization constant (determined from the P_0 fit to the ρ resonance assuming 100% elasticity);

$q = \sqrt{\frac{1}{4} m_{\pi\pi}^2 - m_\pi^2}$, where m_π = pion mass;

$$\Gamma = \Gamma_R \left(\frac{q}{q_R}\right)^{2J+1} \frac{D_J(q_R r)}{D_J(qr)} ,$$

where

$q_R = q(m_{\pi\pi} = m_R)$

D_J = centrifugal barrier functions,

and J, m_R, Γ_R, and X_R are the spin, mass, width, and elasticity of the resonance in question. The parameter r was left free in the range between 1.0 and 10.0 GeV^{-1} (1 fm $\simeq$ 5 GeV^{-1}). For the D_0-wave we included the isospin I = 2 D-wave. This was assumed to be purely elastic with the phase shifts given by Hoogland et al. [15]. The results of the fit are compared (table 2) with the relevant Particle Data Group [16] values, given in brackets.

The consistency with the previous results is quite good (the large errors for the g resonance are due to the lack of high-mass bins). Since we fit the partial waves obtained from two high-statistics experiments in a model-independent way, our results may well represent the best parameters for the $\rho(770)$ and $f(1270)$ resonances.

Having extracted resonance parameters from the most prominent features of the leading waves, we turn to the lower partial waves in the mass region above 1400 MeV/c^2. As we have already mentioned, it is here that we can distinguish between various solutions obtained in previous studies. Our results show that the S-wave passes through a very low value around 1500 MeV/c^2, and the P_0-wave probably goes through a broad $\rho'(1600)$ resonance while the D_0-wave is of similar strength. As is seen in fig. 3 these features (especially the last one) strongly disfavour the α solution of Martin and Pennington. Our points are fairly well described by the β' solution, but β cannot be excluded. This distinction is of minor importance since, according to the authors, β and β' are "two minima in a fairly shallow plane and not in separated and distinct valleys". It should be

stressed here that we have normalized the $|S|^2 + |P_0|^2 + |D_0|^2$ values, predicted by all solutions, to the experimental sum of the relevant intensities. If we had taken the nominal values, all curves would go up. This would mean even stronger disagreement for the α solution, but β and β' would still have been consistent with our results.

The last remark is even more valid for the comparison with the solutions A, B, C, and D of ref. 4 shown in fig. 4. Here also we reduced the $|S|^2 + |P_0|^2 + |D_0|^2$ before comparison and by a larger amount than was necessary for the α, β, and β' solutions. If the S, P_0, and D_0 waves were too strong, some other waves would have been to weak in old solutions. In the next section we will see that it is the $m = 1$ waves which are now stronger in the mass region under consideration.

Coming back to fig. 4 we see that none of the A, B, C, or D solutions fit the data. The nearest is the B solution, as could be expected since this is the origin of the β solution. However, it predicts too low an S-wave and too high a P_0-wave. The A solution is ruled out by too high a D_0-wave (as is α). For completeness we show the C and D solutions, which until now have been disfavoured only by the $\pi^0\pi^0$ data. It is easily seen that they also disagree with our results. Therefore we solve the old ambiguity, demonstrating the unique solution which is close to β or β'. In section 6 we will see that relative phases confirm this statement.

Let us comment on the fact that our results are closer to β than to B. This means that somehow the imposing of analyticity shifted the solution in the same direction as the additional observables supplied by experiment II. This may also mean that our solution is fairly analytical in the sense demanded by Martin and Pennington.

Concluding this section, let us comment on lower partial waves.

The D_0-wave is well described by the f(1270) resonance alone. The fit is only slightly improved ($\chi^2 = 5.5/9$) if we add a higher D-wave resonance. It could be an f'(1520) resonance, but the parameters of this object (if it exists in our results) are very badly determined so we cannot make any conclusive statement.

The f'(1520) would probably be generated via a non-π exchange in order to avoid the Zweig rule ban in the production process. In this context it is interesting to note that the main p_M^L moments, i.e. p_0^0, p_0^2, p_0^4 and p_0^6, all change rapidly around 1500 MeV/c^2. If this effect is significant it could indicate that the production mechanism of the $m_{\pi\pi}$ = 1500 MeV/c^2 object is different from all other objects in the whole mass range.

The P_0 intensity does not represent a strong argument in favour of the $\rho'(1600)$. On the other hand, this resonance is an essential feature of the β-type solution, which our results favour. Therefore this wave has been tentatively fitted by the Breit-Wigner formula in the mass region above 1380 MeV/c^2 using those solutions denoted by full circles in figs. 3 and 4. The results are also shown in table 2.

Finally, the S-wave is certainly very complicated, showing first a maximum at 800 MeV/c^2, an ambiguity at (800-900) MeV/c^2, then a dip at 1000 MeV/c^2, and a broad bump abruptly terminated at 1500 MeV. We shall come back to the S-wave after presenting the phases that are consistent with the narrow $S^*(993)$ and broad $\varepsilon(1200)$ states. Here we will only mention that the rapid fall of the S-wave intensity at 1500 MeV/c^2 may indicate the presence of another object interfering with the tail of the $\varepsilon(1200)$ resonance. The need for many S-wave objects has been voiced for a long time; recently, Robson [17] argued in favour of glueballs in this wave.

5. NON-π EXCHANGE

It has been widely assumed that at low momentum transfer, π exchange is by far the dominating mechanism of our reaction. Experiment II enables us to investigate the other exchanges in a model-independent way; namely, we can determine both the exact amount of the m = 1 waves and the deviation of the m = 0 waves from pure π exchange.

The intensities of m = 1 waves are also shown in fig. 2. Their main features are as follows:

i) they are noticeable only if the relevant m = 0 wave is resonating;

ii) their relative strength decreases with increasing mass (only P_U- and P_N-waves clearly resonate, D_U- and D_N-waves are consistent with resonance behaviour, while the F_U- and F_N-waves are hardly visible);

iii) the natural (e.g. A_2) exchange is roughly of a strength equal to that of the unnatural m = 1 exchange, as was already deduced from the vanishing m = 2 moments.

The so-called "Poor Man's Absorption Model" of Williams [18] predicts the following relation between the unnatural exchange amplitudes:

$$\frac{|L_U|}{|L_0|} = \frac{c_A^L}{m_{\pi\pi}} \sqrt{L(L+1)} \ ,$$

where $|L_U|^2 = (d^2\sigma/dtdm)(|{}^U g_1^1|^2 + |{}^U h_1^1|^2)$ and c_A^L is an absorption constant. It has been found in previous studies [2-4] that c_A^L is independent of L but decreases with the increasing $m_{\pi\pi}$.

In fig. 5 we show the ratio $|L_U|/[|L_0|\sqrt{L(L+1)}]$ as a function of $m_{\pi\pi}$ for our results. It is immediately seen that this function may be fairly complicated. The $m_{\pi\pi}^{-1}$ dependence (normalized in the ρ region) is obviously too weak, thus confirming the above-mentioned trend of the absorption constant. On the other hand, the analysis of Estabrooks and Martin [4] clearly underestimated the amount of the m = 1 unnatural spin-parity exchange, especially above 1400 MeV/c^2. Consequently, the natural exchange was also underestimated. Underestimation of the m = 1 amplitudes is equivalent to overestimation of the S, P_0, and D_0 intensities mentioned in the previous section. The leading F_0-wave is probably so fixed by the t_0^5 and t_0^6 moments that it does not have much freedom. This is confirmed by the value of the g(1690) elasticity remaining unchanged (see table 2).

Now let us discuss the leading m = 0 waves. Pion exchange corresponds to a spin-flip amplitude with m = 0. As we have already observed in section 2, the polarization effect seen in the p_M^L moments shows a significant spin non-flip component in the leading waves (the m = 1 moments are too weak to be responsible

for this effect). We cannot determine this component exactly without the (unknown) phase between the g and h amplitudes. However, we can find its lower limit by exploring the difference between $|g_0^\ell|$ and $|h_0^\ell|$. In the absence of the spin non-flip helicity amplitude the moduli of both transversity amplitudes should be equal. Figure 6 shows that this is not the case in a wide range of $m_{\pi\pi}$ for S-, P_0-, and D_0-waves.

First let us comment on the errors of the $|g_0^\ell|/|h_0^\ell|$ ratio. These errors (being mainly determined by the errors of the p_0 moments) are larger than the errors of intensities (mainly constrained by the t_M^L moments). Apart from increasing with increasing $m_{\pi\pi}$, these errors are large around 1000 MeV/c^2, thus reflecting the minimum in the number of observed events. Taking this into account we can state that there is a general difference between the g and h amplitudes. The latter is usually larger and therefore its phase (see next section) is better determined. This effect decreases with increasing mass. The lower limit of the spin non-flip amplitude can be determined from the formula

$$|n_0^\ell|_{min} = \frac{\left| |g_0^\ell| - |h_0^\ell| \right|}{\sqrt{2}} ,$$

which yields a non-flip/flip ratio of 28% for the $\rho(770)$, 16% for the f(1270), and probably less than 10% for the g(1690). The above fractions represent the minimal amount of the non-π m = 0 exchange. This lower limit is realized when spin-flip and non-flip amplitudes are 90° out of phase (see ref. 11).

Considering also the m = 1 unnatural spin-parity exchange discussed above, we can state that π exchange dominance is weaker than was thought previously. This exchange becomes more dominant with increasing $m_{\pi\pi}$. Especially at lower $m_{\pi\pi}$ there is a considerable amount of exchange with quantum numbers of the A_1. We already know that assumption (a) of the introduction (vanishing of the spin non-flip amplitudes) is no longer valid. However, Ochs [2] has shown that this assumption can be replaced by a weaker one, leaving the old $\pi\pi$ phase shifts unchanged. Namely, it is sufficient to assume that

a′) the spin non-flip amplitudes are proportional to the relevant spin-flip amplitudes with a complex constant independent of $m_{\pi\pi}$ and (ℓ,m) at least for the unnatural exchange.

This assumption translated into the language of transversity amplitudes is equivalent to the following relation (see ref. 11 for a detailed discussion of this topic):

$$|{}^{U}g_{m}^{\ell}|/|{}^{U}h_{m}^{\ell}| = \alpha$$

$$\arg|{}^{U}g_{m}^{\ell}| - \arg|{}^{U}h_{m}^{\ell}| = \delta \ ,$$

where α and δ are independent of ℓ, m, and $m_{\pi\pi}$. In fig. 6 we see that the $|{}^{U}g_{0}|/|{}^{U}h_{0}|$ value slowly increases with $m_{\pi\pi}$. Also, as shown in ref. 11, α for the S-wave is larger than α for the P_0-wave in the ρ region. The second relation deals with the unknown phase δ between the g and h amplitudes. However, if this phase does not depend on the wave, then the relative phase between any g amplitudes must be equal to the relative phase between the relevant h amplitudes. In the next section we will see that this is not exactly true.

6. THE RELATIVE PHASES BETWEEN THE TRANSVERSITY AMPLITUDES

In this analysis, phases provide less information than the intensities. Firstly, we can calculate only the relative phases in a model-independent way. Secondly, these phases are calculated for each transversity separately so that the errors are large. This is particularly so if the moduli of the amplitudes are small. Consequently the errors of the phases between the h amplitudes are usually smaller than those between the g amplitudes. Thirdly, all the relative phases within each transversity set can be multiplied by (-1). When plotting the phases, we select the possibility closer to the old results. Finally, the phases between the transversity amplitudes are not necessarily equal to the phases between the relevant helicity amplitudes. This is only true if assumption (a′), discussed in the previous section, is valid.

We start the presentation with the S-P_0 phase (see fig. 7). At low mass this phase is small, i.e. the S-wave follows the P_0-wave which increases towards the

$\rho(770)$ resonance. Starting from the $\rho(770)$ there is a difference between the two transversity amplitudes. The $g_S - g_0^P$ phase is small and becomes slowly negative to $-(50\text{-}60)^\circ$ around (1200-1400) MeV/c^2 with a possible discontinuity around (900-1100) MeV/c^2. The $h_S - h_0^P$ phase behaves in a similar way above 1000 MeV/c^2, exhibiting the discontinuity at (900-1020) MeV/c^2. This rapid variation of the phase (the P_0 phase should change only slowly by now) together with the drop in the S-wave intensity represents an argument in favour of the $S^*(993)$. But the main feature of the h_S amplitude is the ambiguity between 750 MeV/c^2 and 900 MeV/c^2. This ambiguity resembles the "up-down" ambiguity which was apparently solved by the $\pi^0\pi^0$ data [19] in favour of the "down" solution. The features of this solution are the strong S-wave up to 900 MeV/c^2, relatively large phase (-40°) between the S and P_0, and the 180° phase between the P_U and P_0 amplitudes in fig. 8 (phase coherence). The "up" solution is characterized by the S-wave following the P_0-wave, both in intensity as well as in phase and no phase coherence. It can be seen in fig. 7 that our results do not give a clear answer to this ambiguity (the curves are from Estabrooks and Martin [20]). Let us recall that the "up" solution gives an $\varepsilon(800)$ S-wave resonance. This resonance is preferred to the $\varepsilon(1200)$ by the four-quark speculations (see, for example, Jaffe [21]).

Above 1150 MeV/c^2 the S-P_0 phase stays nearly constant at the level of $-(50\text{-}70^\circ)$. Since the P_0 phase should be nearly constant far above the $\rho(770)$ and well below the possible $\rho'(1600)$, this means that the S amplitude stays near the top of the Argand diagram up to at least 1400 MeV/c^2. This demonstration of a broad $\varepsilon(1200)$ resonance is confirmed by the high intensity of the S-wave (see fig. 2) and the behaviour of the S-D_0 phase (see fig. 9). The latter falls slowly to zero around the f(1270) peak, as is expected for the resonating D_0-wave. Thus we clearly show $\varepsilon(1200)$ in a model-independent way.

The behaviour of the P_0-D_0 phase (also shown in fig. 9) is easily explained by the nearly constant P_0-wave and the resonating D_0-wave, in complete agreement with the intensities of both waves.

The solutions A and B of Estabrooks and Martin [4] as well as α and β of Martin and Pennington are also shown in fig. 9. Even taking into account the sign ambiguity, the B solution can be ruled out, but β (nearly identical to β' in this mass region) is only slightly preferred over α. Although the trend of the g and h phases is the same, the latter are systematically larger.

The same trends are seen in the highest mass region shown in fig. 10. Here the β' solution is clearly favoured by our results. The α solution predicts too high a P_0-F_0 phase, while the β solution gives too high an S-F_0 phase. This means that the S amplitude retains some inelasticity around 1600 MeV/c^2.

For completeness we show (fig. 8) the phases between the unnatural spin-parity exchange amplitudes of the same ℓ. While the phase coherence seems to be in good shape for the P-wave (apart from the "up" version for the h amplitude) there is a definite deviation from this prediction for the D-wave. The sign of each relative phase is fixed by the phase between the leading waves (e.g. the P_0-D_0 phase). Therefore the difference between the g and h amplitudes is quite significant here.

As already stated, the difference between the relative g and h phases means that the unknown phase between the g and h amplitudes is not the same for all waves. In particular the g_U^D-h_U^D phase seems to be different from the others. This in turn means that the weaker assumption (a') of Ochs [2] is not exactly valid. To test this directly we have tried to fit our moments between 1000 MeV/c^2 and 1400 MeV/c^2 assuming

$$U_{n_m}^{\ell} = c_U \, U_{f_m}^{\ell} ,$$

$$N_{n_m}^{\ell} = c_N \, N_{f_m}^{\ell} .$$

The fits are much worse than those for the transversity amplitudes: not only is χ^2/d.f. twice as large, but the results are very unstable even for the intensities, and it is almost impossible to determine the MINOS errors [14] for any parameters. This means that even the weaker assumption (a') is partially broken by the polarized target data (which can be directly deduced from the failure of

the p_M^L moments to be proportional to the t_M^L moments). One of the consequences of this breaking might be the difference between the relative helicity and transversity phases. Therefore the above comparison between our (transversity) results and the old (helicity) phases should be taken with some caution. Nevertheless, the qualitative conclusions should be still valid since the breaking of the weakened assumption (a′) of the introduction seems not to be too strong for the m = 0 waves.

7. THE BARRELET ZEROS OF TRANSVERSITY AMPLITUDES

The $\pi\pi$ scattering amplitude can be written as follows ($\ell_{max} = 3$):

$$A(m_{\pi\pi}, z = \cos\theta) = S + \sqrt{3}\, P_0 z + \sqrt{5}\, D_0\left(\frac{3}{2} z^2 - \frac{1}{2}\right) + \sqrt{7}\, F_0\left(\frac{5}{2} z^3 - \frac{1}{2} z\right)$$

$$= c \prod_{i=1}^{3} (z - z_i) ,$$

where c and z_i are complex functions of $m_{\pi\pi}$. From the experimental cross-sections we determine only the modulus of the amplitude:

$$\frac{d\sigma_{\pi\pi}}{dt} \propto |A(m_{\pi\pi}, z)|^2 = |c|^2 \prod_{i=1}^{3} \left[(z-z_i)(z-z_i^*)\right] = |c|^2 \prod_{i=1}^{3} \left[(z-\mathrm{Re}\, z_i)^2 + |\mathrm{Im}\, z_i|^2\right] .$$

The Barrelet ambiguity is just the uncertainty in the sign of the imaginary parts of the complex zeros since the $\pi\pi$ cross-section is invariant under $z_i \leftrightarrows z_i^*$. Therefore an eightfold ambiguity would be expected. Fortunately each new zero (the zeros are numbered according to the increasing real part) must enter the physical region with a negative imaginary part. On the other hand, whenever Im z_i reaches zero a new ambiguity appears, as it can become either positive or negative.

The results of the previous studies [3,4] can be summarized as follows: in the ρ region Im $z_1 \approx 0$, which produces the first ("up-down") ambiguity apparently solved by the $\pi^0\pi^0$ data [19]. Around 1200 MeV/c^2, Im z_1 (the first zero is the one with Re $z_1 < 0$) goes through zero again. This is the origin of the main ambiguity (A or B). At $\sim$ 1450 MeV/c^2, Im $z_2 \approx 0$ (the second zero has small positive real part) thus producing four solutions (A → A,C; B → B,D). The imaginary part

of the third zero (large positive real part) vanishes only at 1800 MeV. Many ambiguities would be expected above this mass, since here also Im $z_1 \approx 0$, but this is irrelevant for the present work. The standard procedure of finding new solutions was to calculate the Barrelet zeros of the old solution, then to flip the signs of the imaginary parts, next to calculate the new partial waves, and finally to use them as the starting values for the fitting program. The need for refitting is due to the non-π exchange contribution to the measured moments. If it were strong enough, one would hope to distinguish between the various solutions.

Our analysis has already shown that the non-π exchange terms are stronger than was thought previously. Also, we have found a unique solution above 1000 MeV/c^2 (except for some ambiguities around 1500 MeV/c^2), even though various independent starting points were used for the fit. Thus it could be expected that the Barrelet zeros for our transversity amplitudes differ considerably from the old results.

We see that this is the case when comparing the zeros of Estabrooks and Martin [4] with our results. In fig. 11 the imaginary parts fluctuate around the zero value (of course apart from the initial region in which their sign is fixed). These fluctuations are larger for the g amplitude than for the better determined h amplitude. There are some deviations (Im $z_{1,2} \neq 0$) around 1500 MeV/c^2 and they produce large ambiguities, but otherwise Barrelet zeros produce no ambiguity. The real parts of the Barrelet zeros are just the positions of the minima of the amplitude as a function of $z = \cos\theta$. Here we do not see any significant deviation from the results of ref. 4; there are only fluctuations, especially for the g amplitude between 1300-1600 MeV/c^2. The vanishing of the imaginary parts means that the amplitude goes right down to zero in the minima for nearly the whole mass range above 1100 MeV/c^2.

8. CONCLUDING REMARKS

In this analysis we have used the results of experiment I on the reaction

$$\pi^- p \to \pi^+ \pi^- n \text{ at } 17.2 \text{ GeV/c} ,$$

which were the basis of the previous studies [2-4,8,9]. Consequently our results could not be entirely different from the results of those studies. However, the polarized target experiment allows us to perform a completely model-independent analysis, thus testing the quality of the assumptions made previously. This does not mean that we could determine all the parameters of the partial waves. Owing to the lack of measurement of the recoil polarization, we have been forced to use transversity amplitudes, which restricts the possibility of direct comparison with previous results. We have favoured this procedure rather than introduce any physical assumption. Also, we have performed an energy-independent analysis not providing absolute phases. Determination of phase shifts would need some fixing of the over-all phase by demanding the Breit-Wigner formulae for the leading waves and some additional theoretical input, e.g. by imposing analyticity.

Using our approach we have found a unique solution for the partial waves, thus solving the old ambiguities. The uniqueness of the solution is confirmed by the Barrelet-zeros analysis. The solution is close to the analytical β' solution of Martin and Pennington. Further, we have determined the exact amount of each partial wave, which enables us to find the resonance parameters and to show that the non-π exchange is stronger than has been thought in the low four-momentum transfer region. This effect is present even in the leading $m = 0$ waves but decreases with increasing mass. The separation of non-π exchange into A_1 exchange and absorptive cuts probably needs a model-dependent analysis as in refs. 12 and 22.

The study of resonances in our data needs further effort. In particular, the complicated structure of the S-wave represents a real challenge. The interest in this wave has recently been stirred by glueballs [17] and $q\bar{q}q\bar{q}$ systems [21].

Acknowledgements

The authors profited very much from numerous discussions with Drs. K. Fialkovski, W. Ochs, M.R. Pennington and F. Wagner. Their suggestions, comments, and criticism were very fruitful for this work.

Some of us would like to express their gratitude to CERN (K.R.) and to the Max Planck Institute (J. de G., B.N. and T.P.) for the support and hospitality during the experiment and analysis.

REFERENCES

[1] G. Grayer et al., Nuclear Phys. B75 (1974) 189.

[2] W. Ochs, Thesis, Ludwig Maximilians Universität, Munich, 1973.
B. Hyams et al., Nuclear Phys. B64 (1973) 134.

[3] W. Männer, Proc. 4th Internat. Conf. on Experimental Meson Spectroscopy, Boston, 1974 (American Institute of Physics, New York, 1974), p. 22.
B. Hyams et al., Nuclear Phys. B100 (1975) 205.

[4] P. Estabrooks and A.D. Martin, Nuclear Phys. B95 (1975) 322.

[5] E. Barrelet, Nuovo Cimento 8A (1972) 331.

[6] A. Shimada, Progr. Theor. Phys. 54 (1975) 758.

[7] V.D. Apel et al., Phys. Letters 57B (1975) 398.

[8] C.D. Froggatt and J.L. Petersen, Nuclear Phys. B129 (1977) 89.

[9] A.D. Martin and M.R.Pennington, CERN preprint TH-2353 (1977).

[10] H. Becker et al., Proc. 18th Internat. Conf. on High-Energy Physics, Tbilisi, 1976 (JINR, Dubna, 1976), p. 27.

[11] H. Becker et al. (submitted to Nuclear Physics).

[12] J. de Groot, Thesis, Amsterdam University, 1978.

[13] G. Lutz and K. Rybicki, MPI report MPI-PAE/Exp.EL.75 (October 1978).

[14] F. James and M. Roos, Comput. Phys. Commun. 10 (1975) 343.

[15] W. Hoogland et al., Nuclear Phys. B126 (1977) 109.

[16] Particle Data Group, Rev. Mod. Phys. 48 (1976) No. 2, part II.

[17] D. Robson, Nuclear Phys. B130 (1977) 328.

[18] P.K. Williams, Phys. Rev. D1 (1970) 1312.

[19] V.D. Apel et al., Phys. Letters 41B (1973) 542.

[20] P. Estabrooks and A.D. Martin, Nuclear Phys. B79 (1974) 301.

[21] R.L. Jaffe, Phys. Rev. D15 (1977) 267.

[22] J.D. Kimel and J.F. Owens, Nuclear Phys. B122 (1977) 464.

Table 1

Fit parameters used in the different mass regions

Highest wave	P	D	F
Mass region (MeV)	580-900	900-1380	1380-1780
No. of amplitudes ($m \leq 1$)	8	14	20
No. of real parameters	14	26	38
No. of moments ($M \leq 2$)	15	31	47
Analytical solution	exact	approximate	approximate
χ^2/d.f.	0.8	0.5	0.8

Table 2

Resonance parameters from fits

Resonance	ρ	f	g	ρ'
Mass (MeV)	776.1 ± 2.6	$1273.8\ ^{+2.8}_{-2.7}$	$1716\ ^{+58}_{-29}$	$1598\ ^{+24}_{-22}$
	(773 ± 3)	(1271 ± 5)	(1690 ± 20)	(1600)
Width (MeV)	$161.8\ ^{+7.6}_{-7.2}$	$183.2\ ^{8.3}_{-7.9}$	$325\ ^{+\infty}_{-119}$	$175\ ^{+98}_{-53}$
	(152 ± 3)	(180 ± 20)	(180 ± 30)	(200-800)
Elasticity (%)	100 (input)	84.7 ± 1.6	$25.9\ ^{+1.8}_{-1.9}$	$28.7\ ^{+4.3}_{-4.2}$
	(100)	(81 ± 1)	(24 ± 1)	(?)
r (GeV^{-1})	5.3	10.0	3.0	1.0
Mass range (MeV)	580-980	980-1660	1420-1780	1420-1780
χ^2/d.f.	8.1/6	11.8/13	2.0/5	5.4/5

Figure captions

Fig. 1a : Uppermost plot: $\pi\pi$ mass distribution in experiment I. Open circles show the raw data, full circles are obtained after the correction for acceptance losses, etc. The errors are always within the size of the circles. Lower plots: mass dependence of the normalized moments p_0^0, t_0^1, and p_0^1 ($t_0^0 \equiv 1/\sqrt{4\pi}$). Errors if not shown are smaller than the size of a circle.

Fig. 1b : Mass dependence of the normalized moments t_0^2, p_0^2, t_0^3, and p_0^3. Errors if not shown are smaller than the size of the circle.

Fig. 1c : Mass dependence of the normalized moments t_0^4, p_0^4, t_0^5, p_0^5, t_0^6, and p_0^6. Errors if not shown are smaller than the size of the circle.

Fig. 1d : Mass dependence of the normalized moments with M = 1: t_1^1, p_1^1, r_1^1, t_1^2, p_1^2, and r_1^2. Errors if not shown are smaller than the size of a circle.

Fig. 1e : Mass dependence of the normalized moments with M = 1: t_1^3, p_1^3, r_1^3, t_1^4, p_1^4, and r_1^4. Errors if not shown are smaller than the size of the circle.

Fig. 1f : Mass dependence of the normalized moments with M = 2: from t_2^2 to r_2^4. Errors if not shown are smaller than the size of the circle.

Fig. 1g : Mass dependence of the normalized moments with $M \geq 1$: from t_1^5 to r_2^6. Errors if not shown are smaller than the size of the circle.

Fig. 2 : Intensities of partial waves in microbarns (without division by the bin size). Full circles show the unique or preferred solution (see text); open circles, possible other solutions. Errors if not shown are smaller than the size of the circles.

Fig. 3 : Comparison of partial wave intensities above 1400 MeV/c^2 with various solutions of Martin and Pennington [9]. Units and conventions are as in fig. 2.

Fig. 4 : Comparison of partial wave intensities with the solutions of Estabrooks and Martin [4]. Units and intensities are as in fig. 2.

Fig. 5 : Mass dependence of the ratio $|L_U|/[|L_0|\sqrt{L(L+1)}]$. In case of ambiguity only the preferred solution is plotted. Values with errors exceeding 100% are not shown. The curve denoted $1/m_{\pi\pi}$ (normalized at the ρ peak) shows the dependence expected from the absorption model if the strength of absorption does not depend on $m_{\pi\pi}$. The curve denoted EM shows the results of Estabrooks and Martin.

Fig. 6 : The ratio of transversity amplitudes with m = 0. Hereafter g_S is a shortened notation for ${}^U g_0^0$, g_P for ${}^U g_0^1$, etc. A deviation from unity shows the strength of non-π exchange.

Fig. 7 : The relative phases between the S and P_0 transversity amplitudes. The open circles for the h amplitude represent the solution more similar to the "up" solution. The curves are from Estabrooks and Martin [20].

Fig. 8 : The relative phases between the unnatural spin-parity exchange transversity amplitudes of the same dipion spin (g_U^P stands for ${}^U g_1^1$, etc.). The open circles for the h amplitude represent the solution that is more similar to the "up" solution. The phase coherence assumption is right if the phase difference is 180°.

Fig. 9 : The relative phases with respect to the D_0 transversity amplitudes between 1140 MeV/c^2 and 1420 MeV/c^2. The curves marked A and B represent the solutions of Estabrooks and Martin [4], α and β those of Martin and Pennington [9].

Fig. 10 : The relative phases with respect to the F_0 transversity amplitudes above 1380 MeV/c^2. In case of ambiguity, open circles represent the disfavoured solution (see end of section 3 for details). The curves show the α, β, and β' solutions of Martin and Pennington.

Fig. 11a : The Barrelet zeros of the transversity-down amplitude g. The full squares (circles) show the real (imaginary) part for the unique or preferred solutions; the open ones, those of the disfavoured solutions (see end of section 3 for details). The curves are after Estabrooks and Martin [4].

Fig. 11b : The Barrelet zeros of the transversity-up amplitude h. The full squares (circles) show the real (imaginary) part for the unique or preferred solutions; the open ones, those of the disfavoured solutions (see end of section 3 for details). The curves are after Estabrooks and Martin [4].

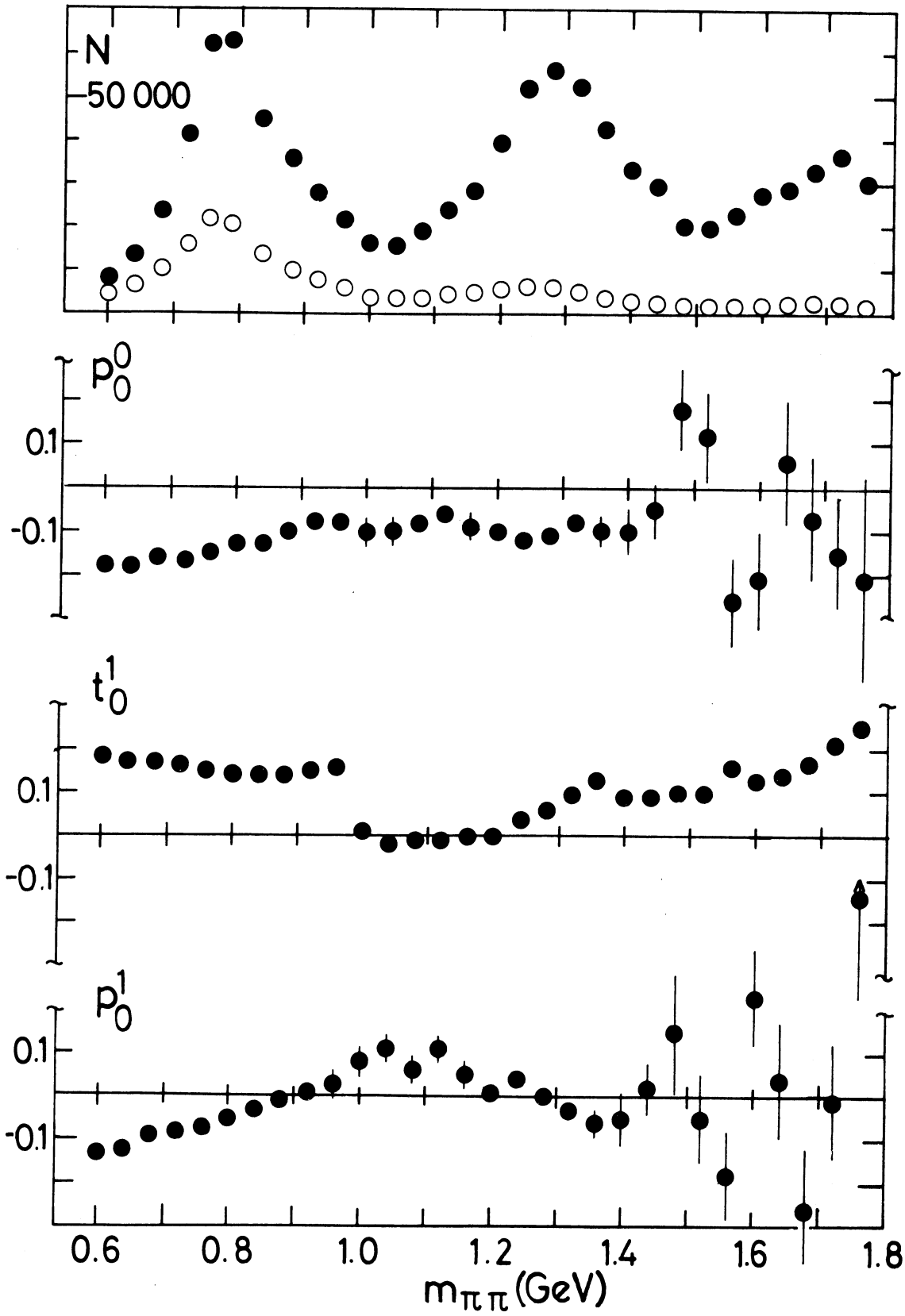

Fig. 1a

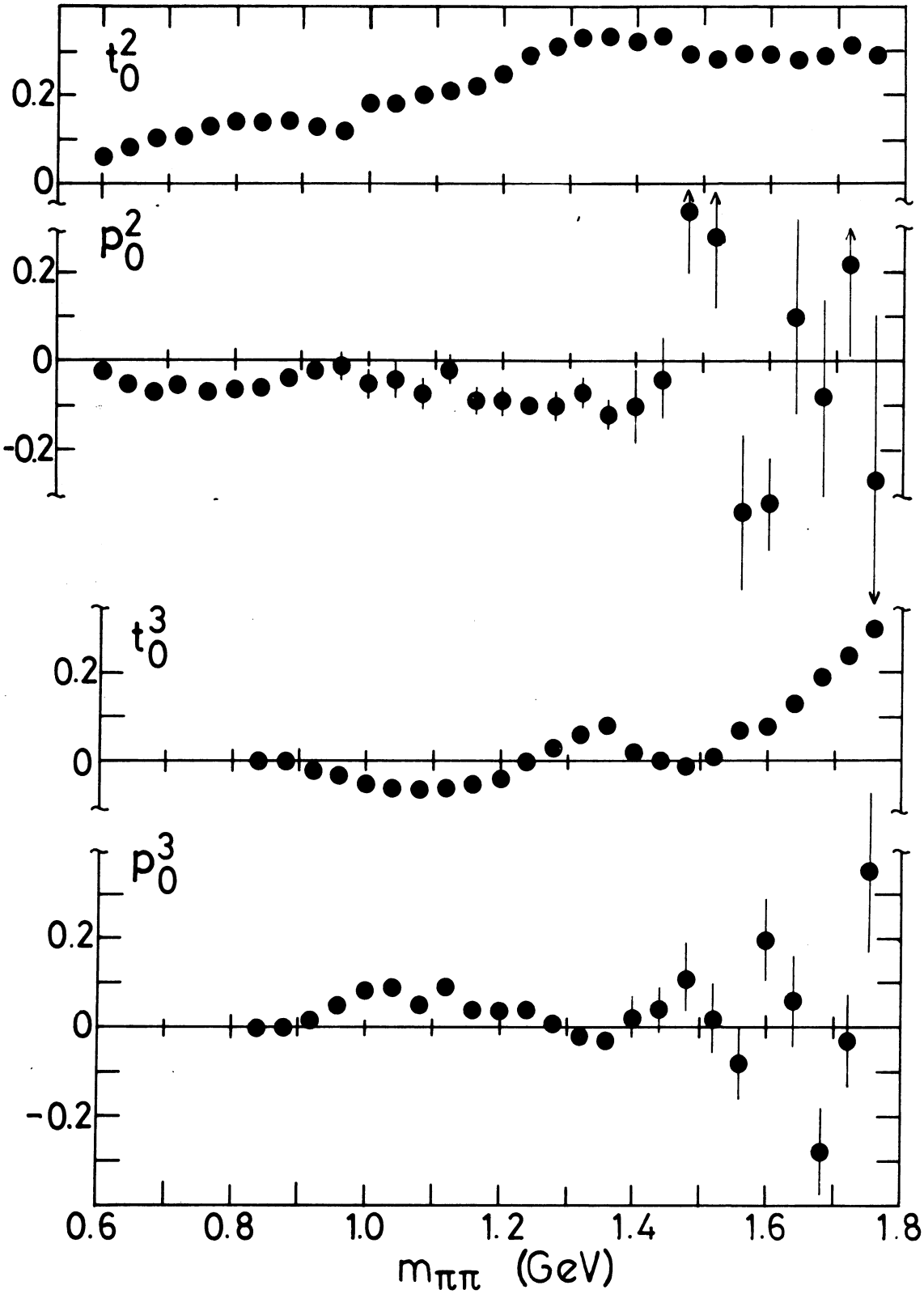
t_0^2
0.2
0
p_0^2
0.2
0
-0.2
t_0^3
0.2
0
p_0^3
0.2
0
-0.2
0.6
0.8
1.0
1.2
1.4
1.6
1.8
$m_{\pi\pi}$ (GeV)

Fig. 1b

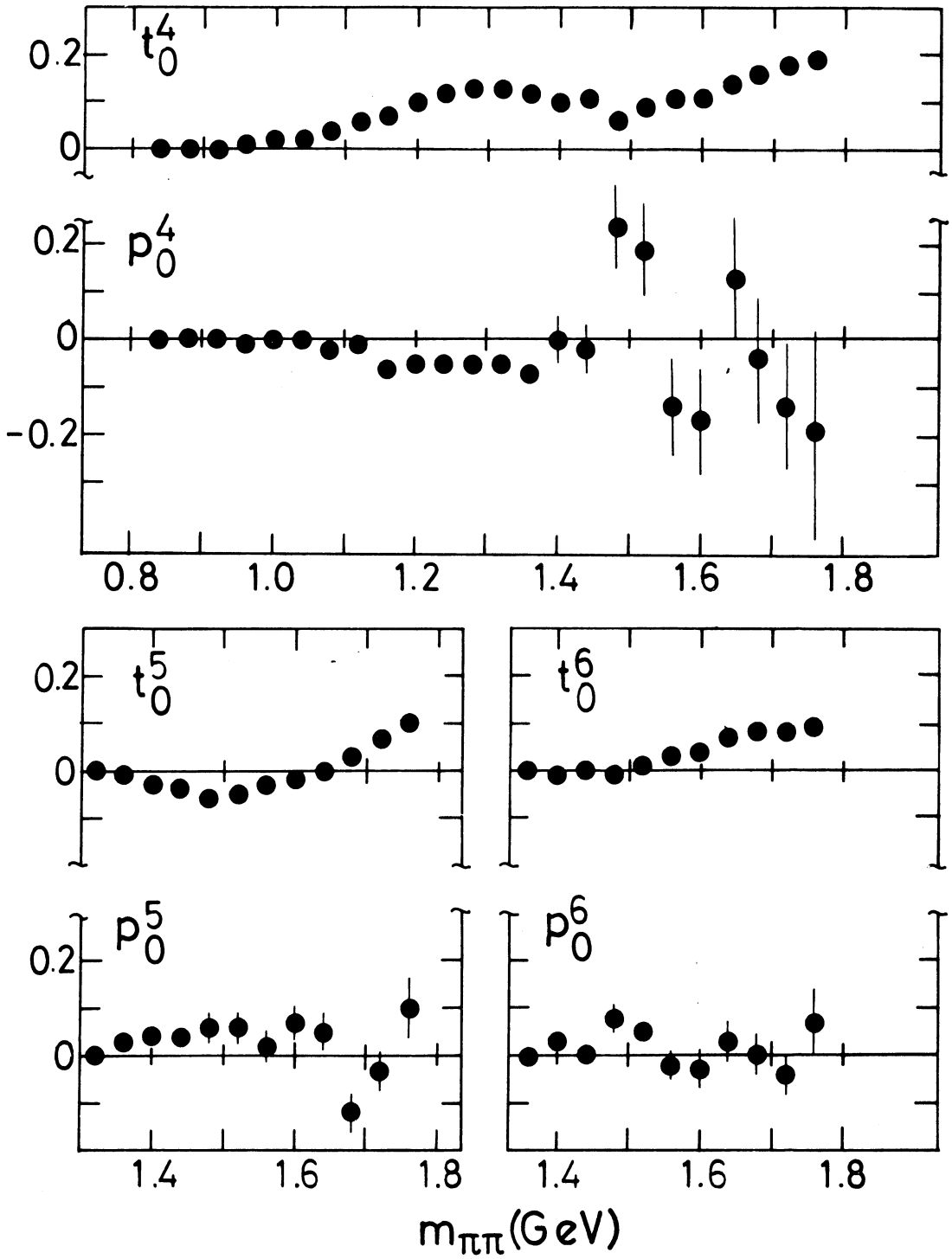

Fig. 1c

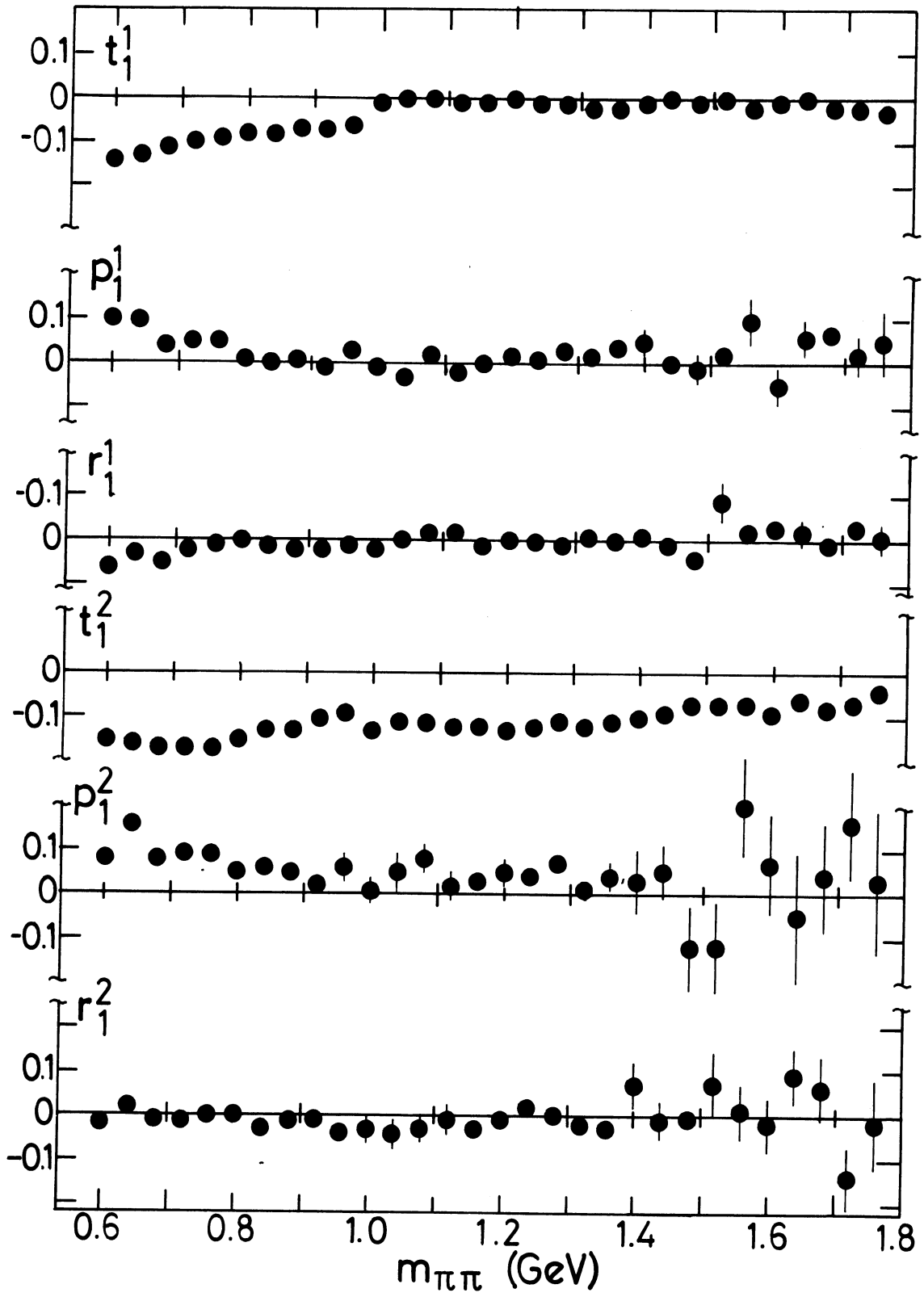

Fig. 1d

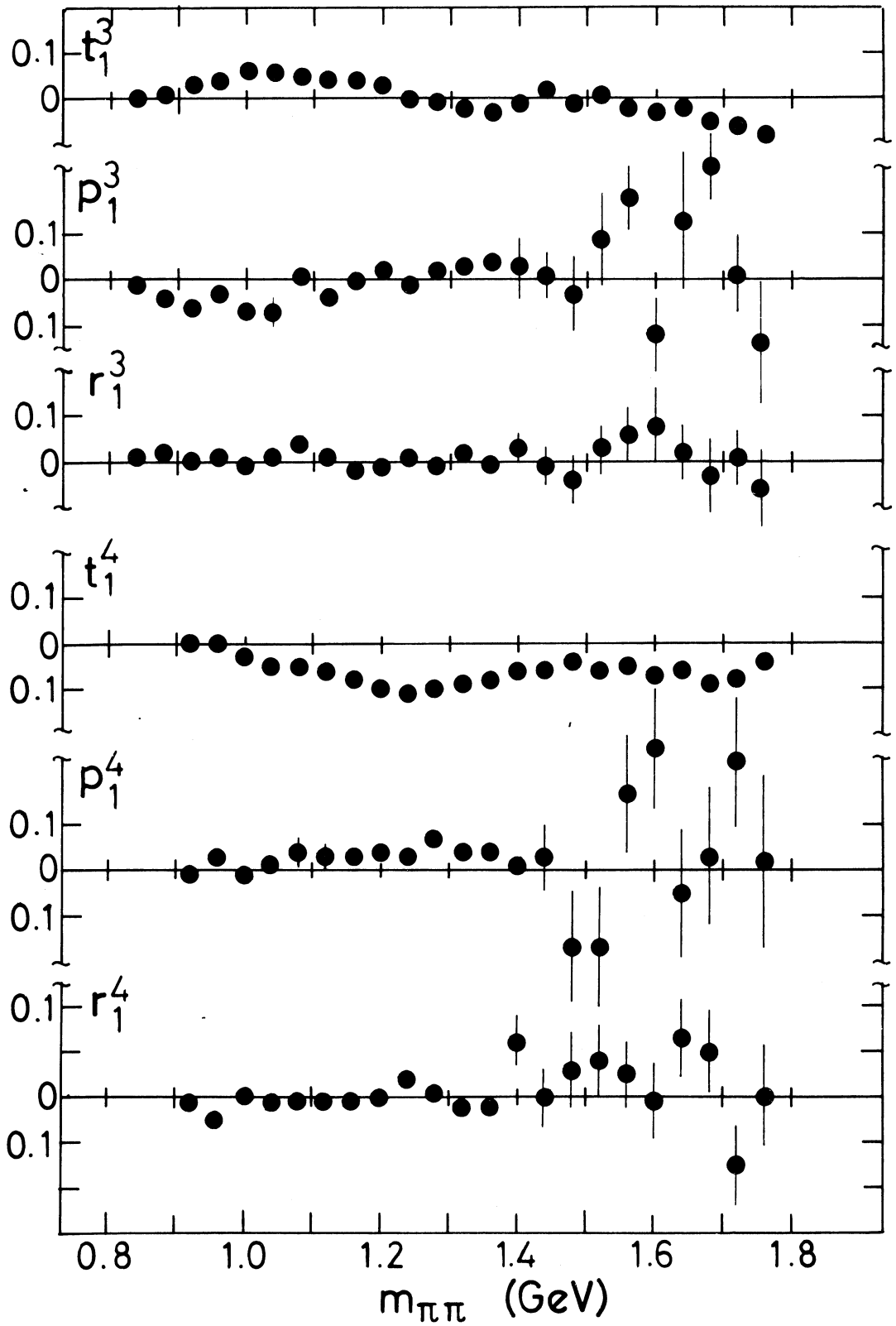

Fig. 1e

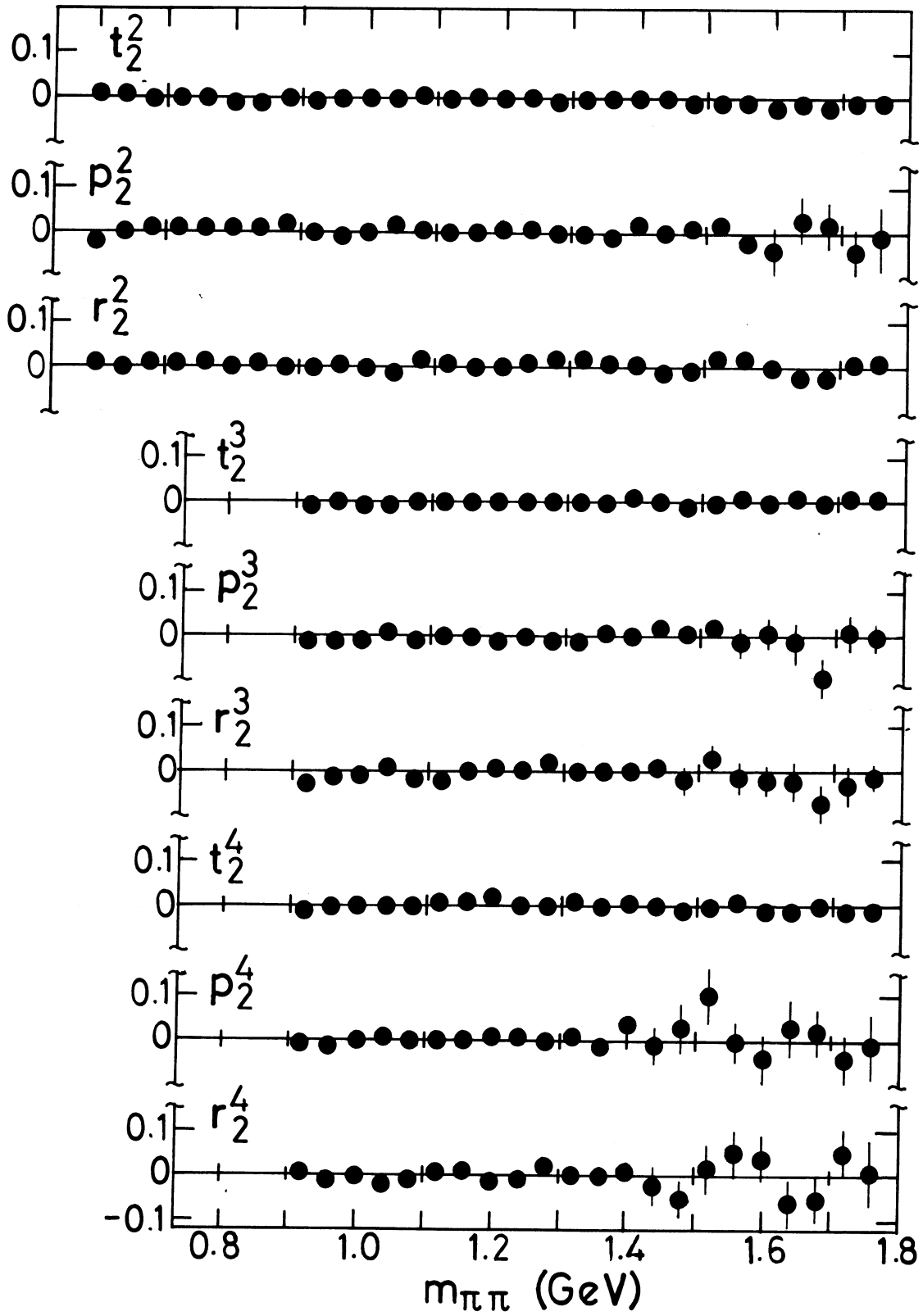
0.1
0
t_2^2
p_2^2
r_2^2
t_2^3
p_2^3
r_2^3
t_2^4
p_2^4
r_2^4
-0.1
0.8
1.0
1.2
1.4
1.6
1.8
$m_{\pi\pi}$ (GeV)

Fig. 1f

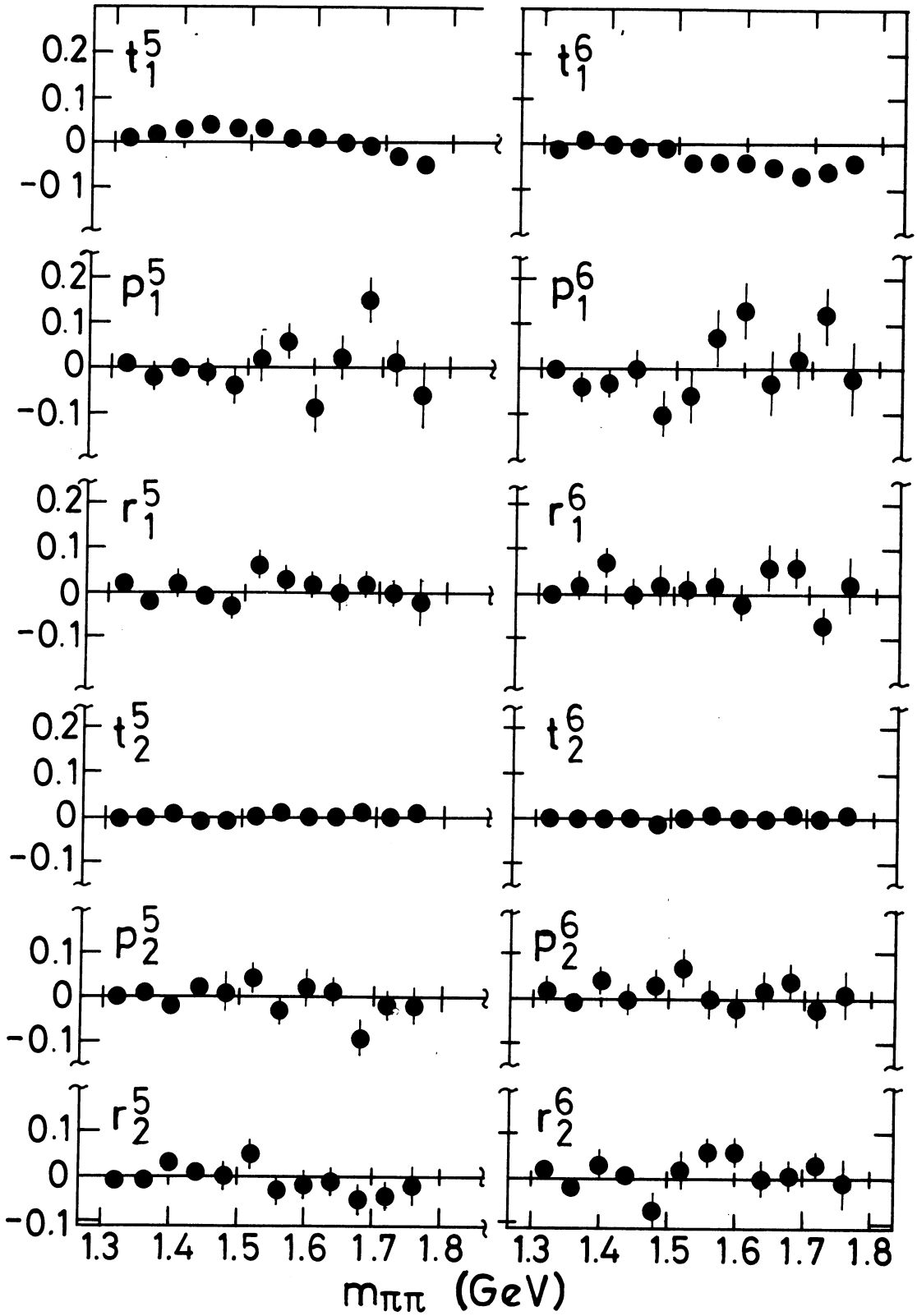
t_1^5
t_1^6
p_1^5
p_1^6
r_1^5
r_1^6
t_2^5
t_2^6
p_2^5
p_2^6
r_2^5
r_2^6
0.2
0.1
0
-0.1
1.3
1.4
1.5
1.6
1.7
1.8
$m_{\pi\pi}$ (GeV)

Fig. 1g

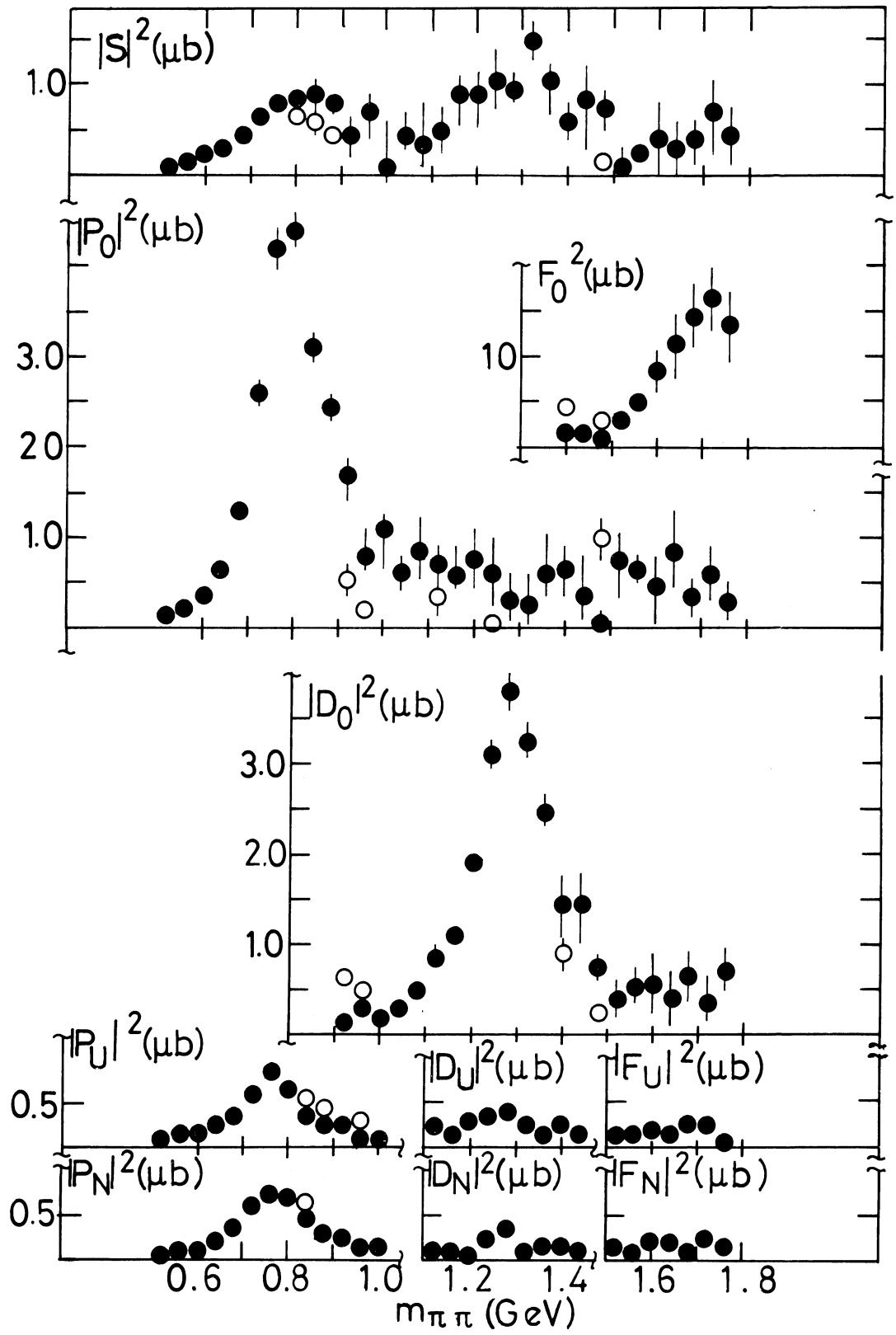
$|S|^2(\mu b)$
1.0
$|P_0|^2(\mu b)$
3.0
2.0
1.0
$F_0{}^2(\mu b)$
10
$|D_0|^2(\mu b)$
3.0
2.0
1.0
$|P_U|^2(\mu b)$
0.5
$|D_U|^2(\mu b)$
$|F_U|^2(\mu b)$
$|P_N|^2(\mu b)$
0.5
$|D_N|^2(\mu b)$
$|F_N|^2(\mu b)$
0.6
0.8
1.0
1.2
1.4
1.6
1.8
$m_{\pi\pi}$ (GeV)

Fig. 2

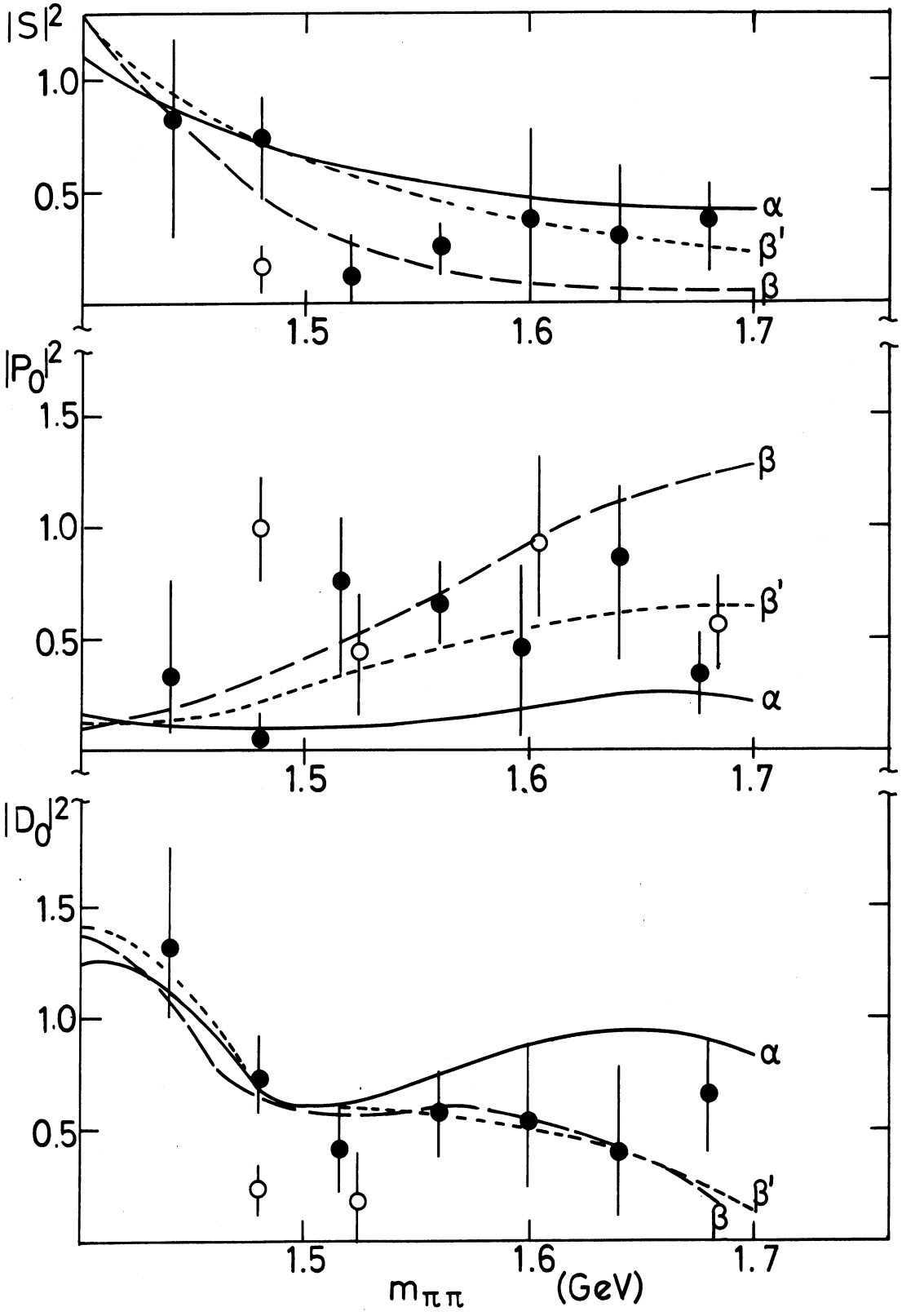
|S|²
1.0
0.5
α
β'
β
1.5
1.6
1.7
|P₀|²
1.5
1.0
0.5
β
β'
α
1.5
1.6
1.7
|D₀|²
1.5
1.0
0.5
α
β'
β
1.5
1.6
1.7
mππ (GeV)

Fig. 3

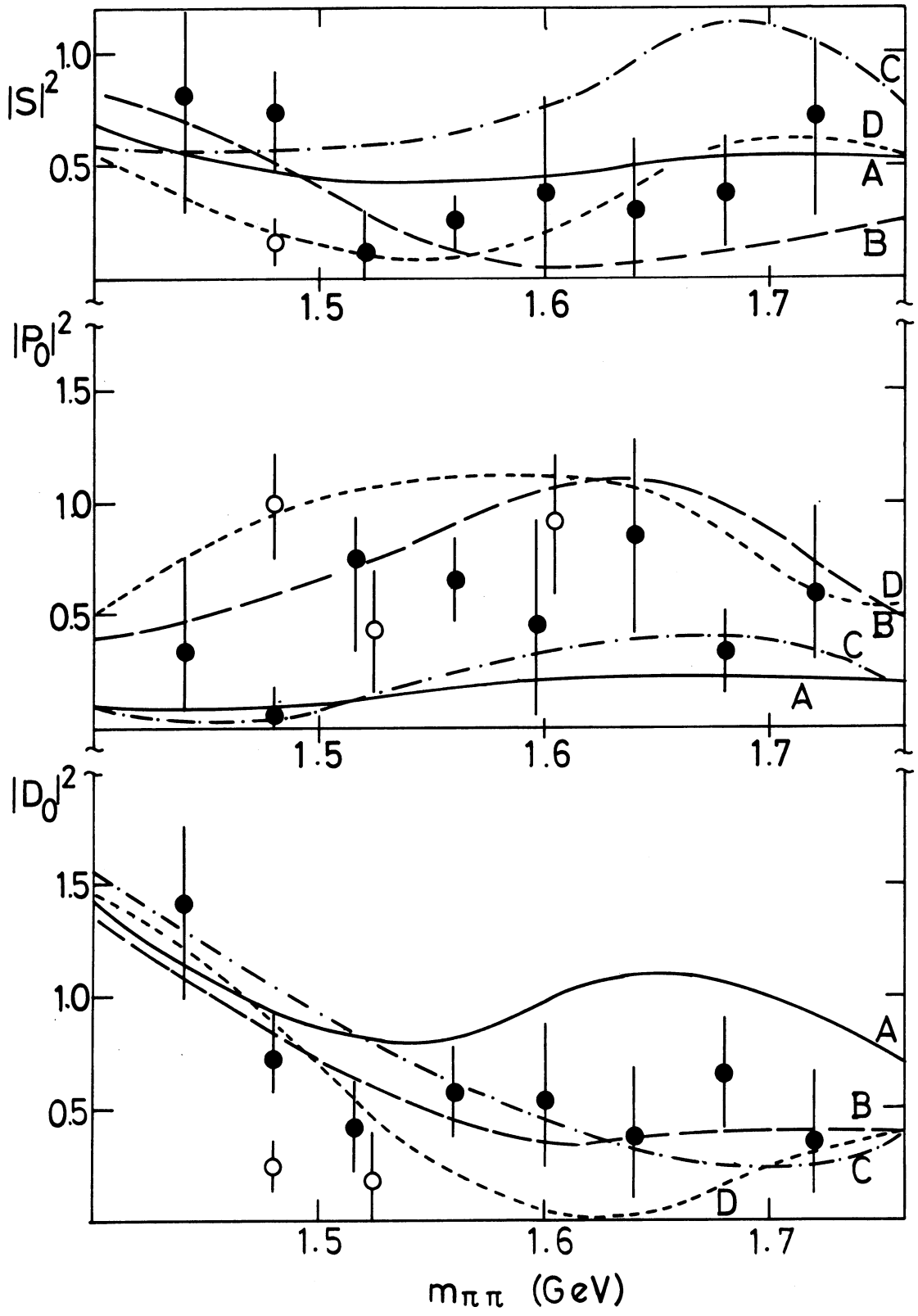
$|S|^2$
1.0
0.5
C
D
A
B
1.5
1.6
1.7
$|P_0|^2$
1.5
1.0
0.5
D
B
C
A
1.5
1.6
1.7
$|D_0|^2$
1.5
1.0
0.5
A
B
C
D
1.5
1.6
1.7
$m_{\pi\pi}$ (GeV)

Fig. 4

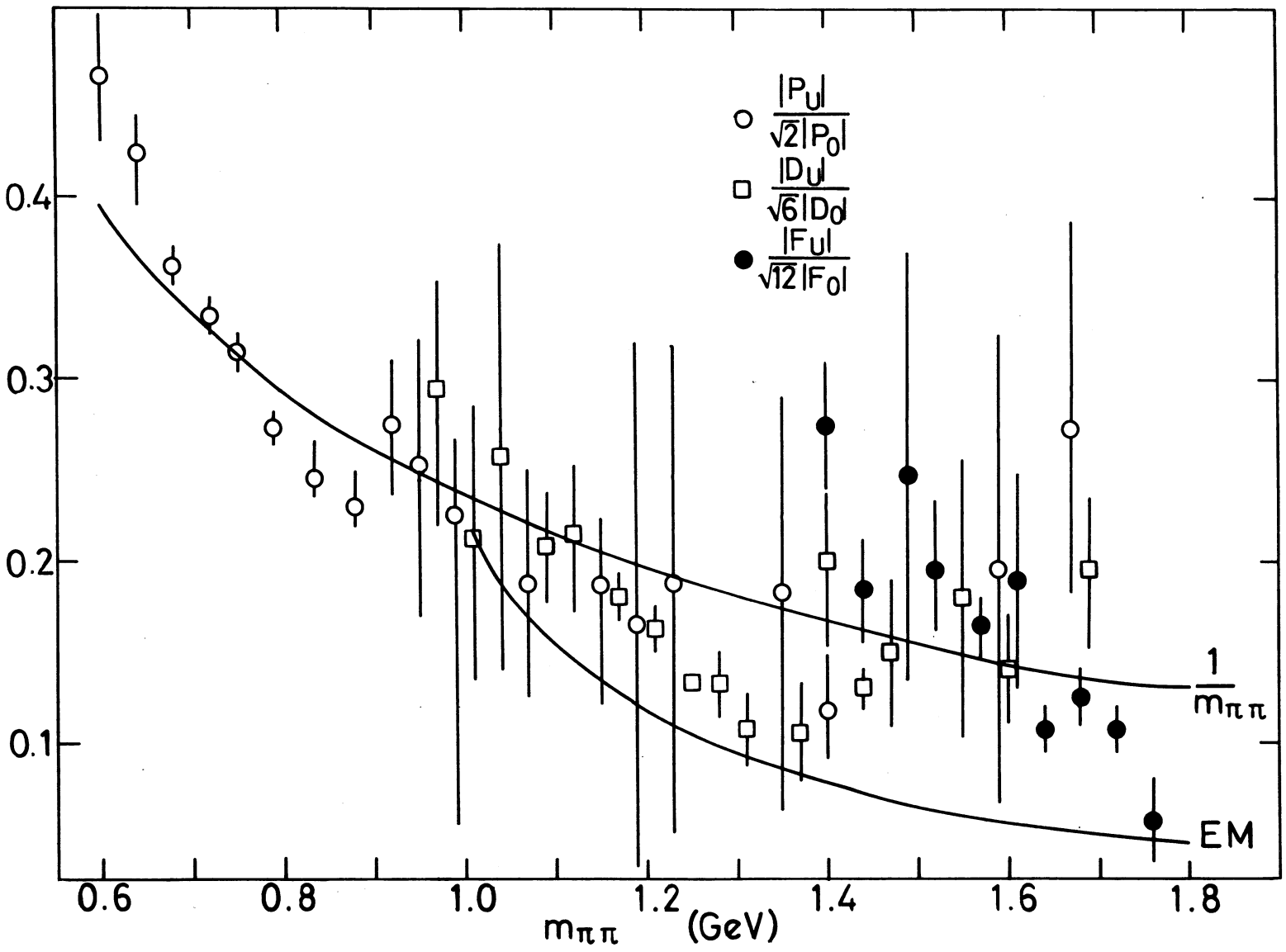
$\frac{|P_U|}{\sqrt{2}|P_0|}$
$\frac{|D_U|}{\sqrt{6}|D_0|}$
$\frac{|F_U|}{\sqrt{12}|F_0|}$
0.4
0.3
0.2
0.1
0.6
0.8
1.0
1.2
1.4
1.6
1.8
$m_{\pi\pi}$ (GeV)
$\frac{1}{m_{\pi\pi}}$
EM

Fig. 5

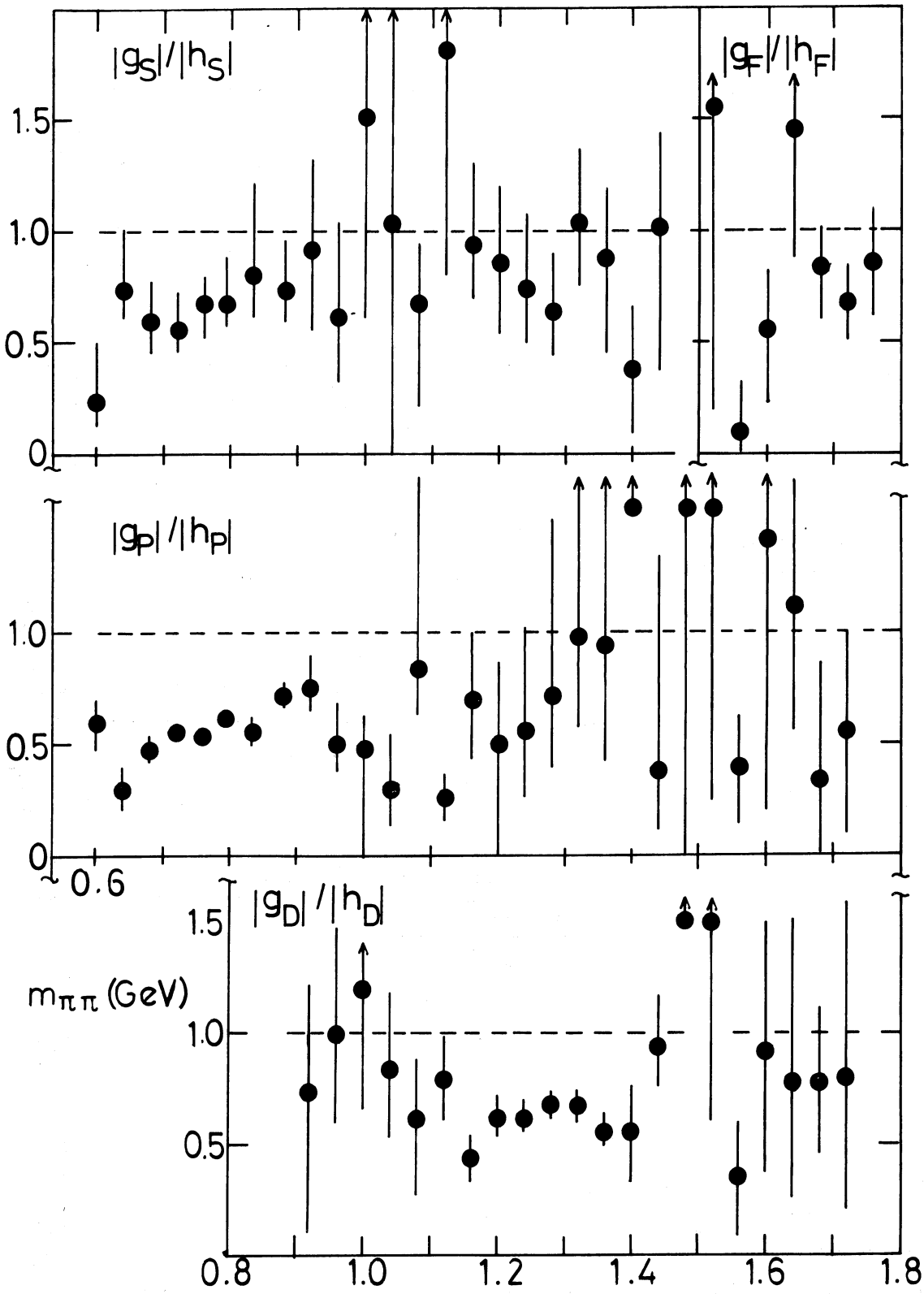

Fig. 6

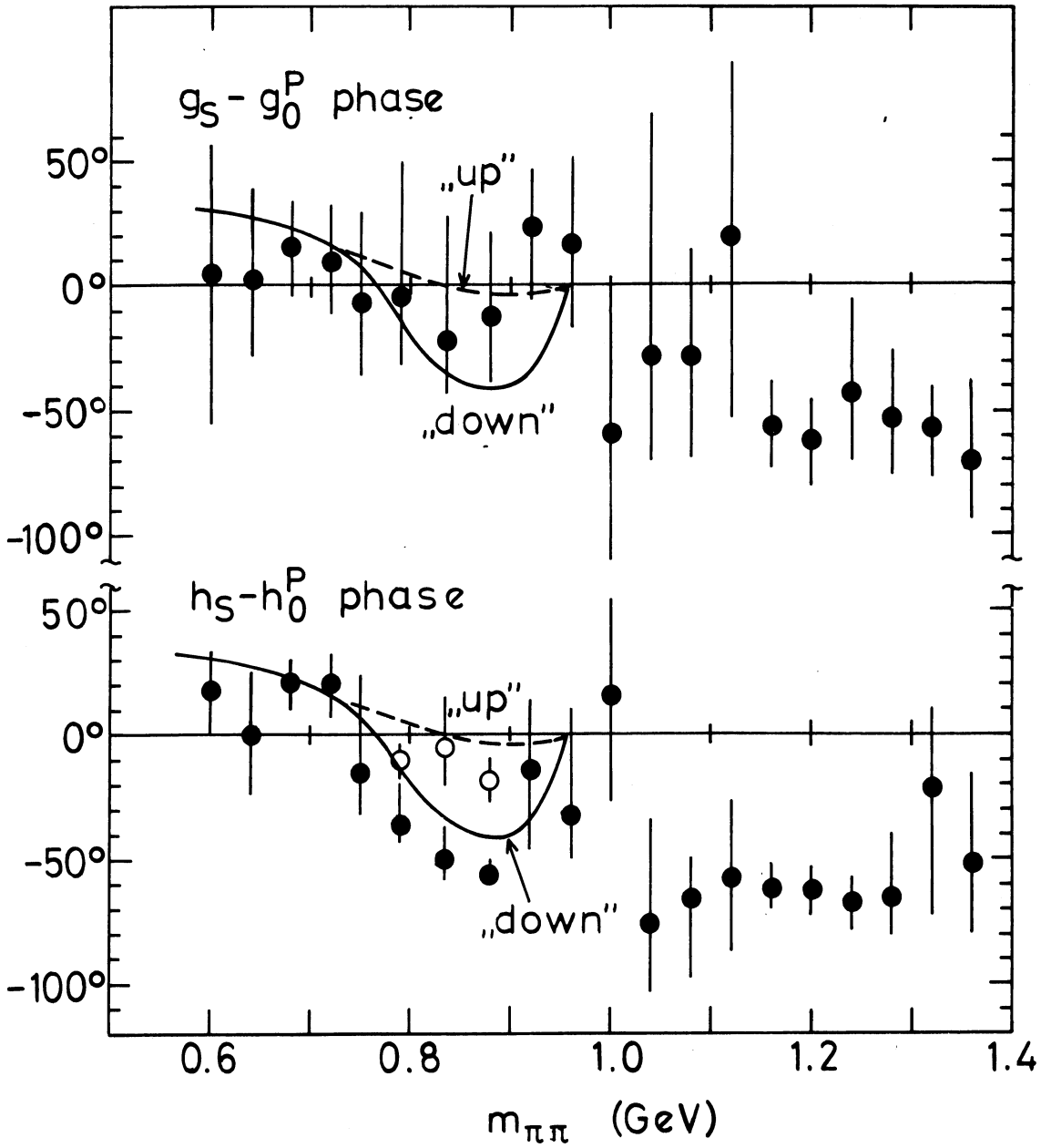
$g_S - g_0^P$ phase
50°
0°
-50°
-100°
„up"
„down"
$h_S - h_0^P$ phase
50°
0°
-50°
-100°
„up"
„down"
0.6
0.8
1.0
1.2
1.4
$m_{\pi\pi}$ (GeV)

Fig. 7

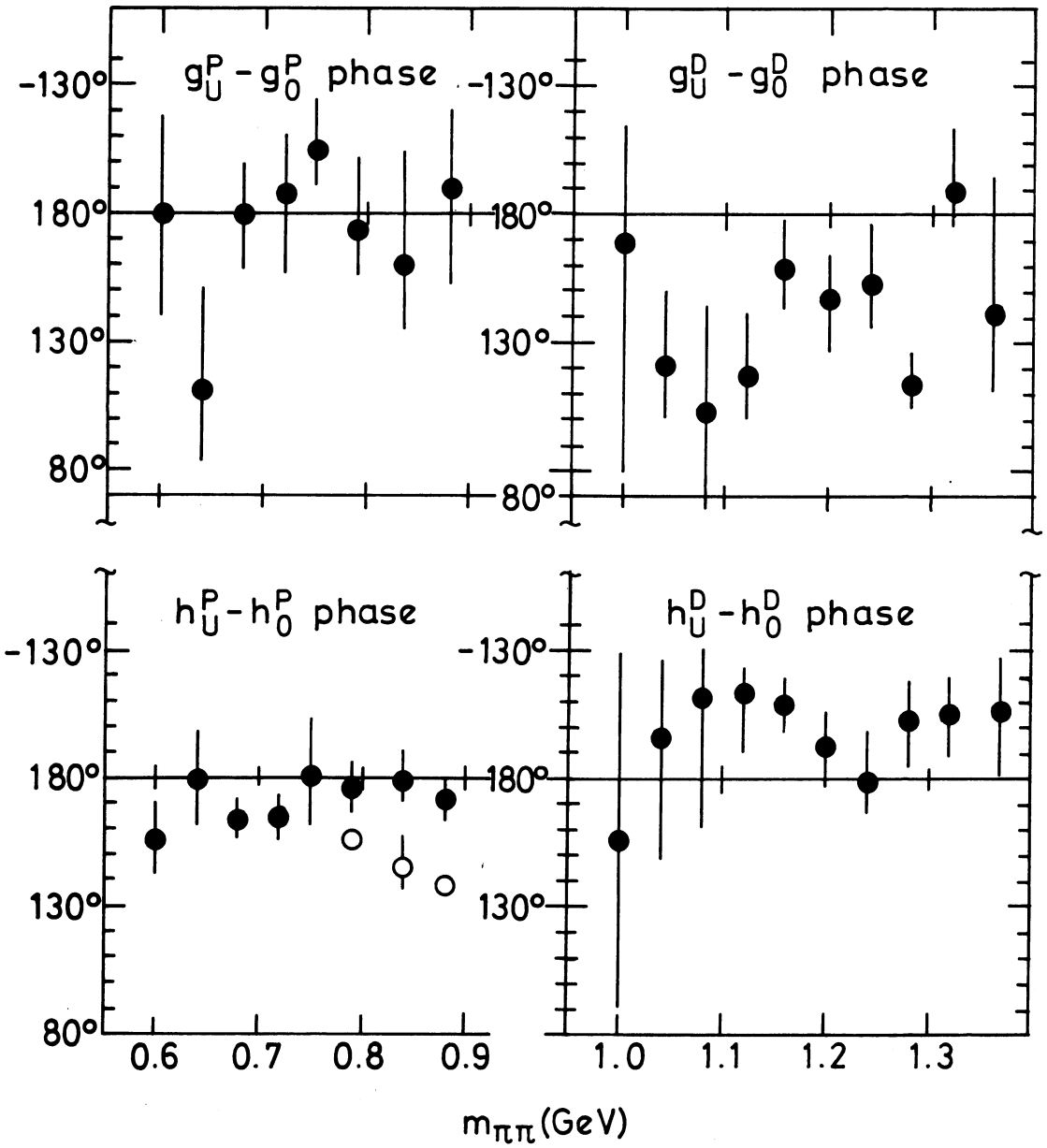
$g_U^P - g_0^P$ phase
$g_U^D - g_0^D$ phase
$h_U^P - h_0^P$ phase
$h_U^D - h_0^D$ phase
-130°
180°
130°
80°
0.6
0.7
0.8
0.9
1.0
1.1
1.2
1.3
$m_{\pi\pi}$(GeV)

Fig. 8

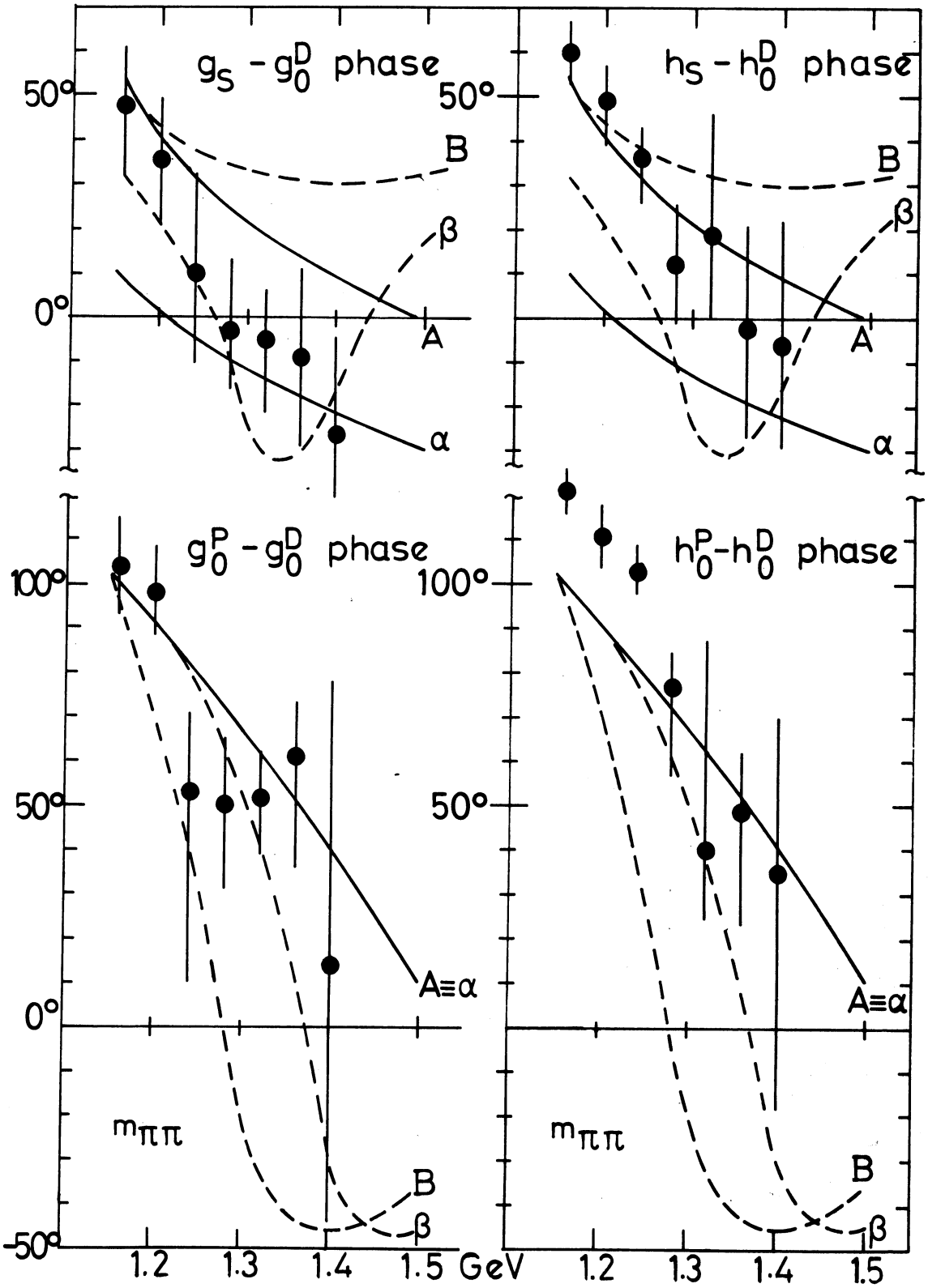
$g_S - g_0^D$ phase
$h_S - h_0^D$ phase
$g_0^P - g_0^D$ phase
$h_0^P - h_0^D$ phase
50°
0°
100°
-50°
B
β
A
α
A≡α
$m_{\pi\pi}$
1.2
1.3
1.4
1.5 GeV

Fig. 9

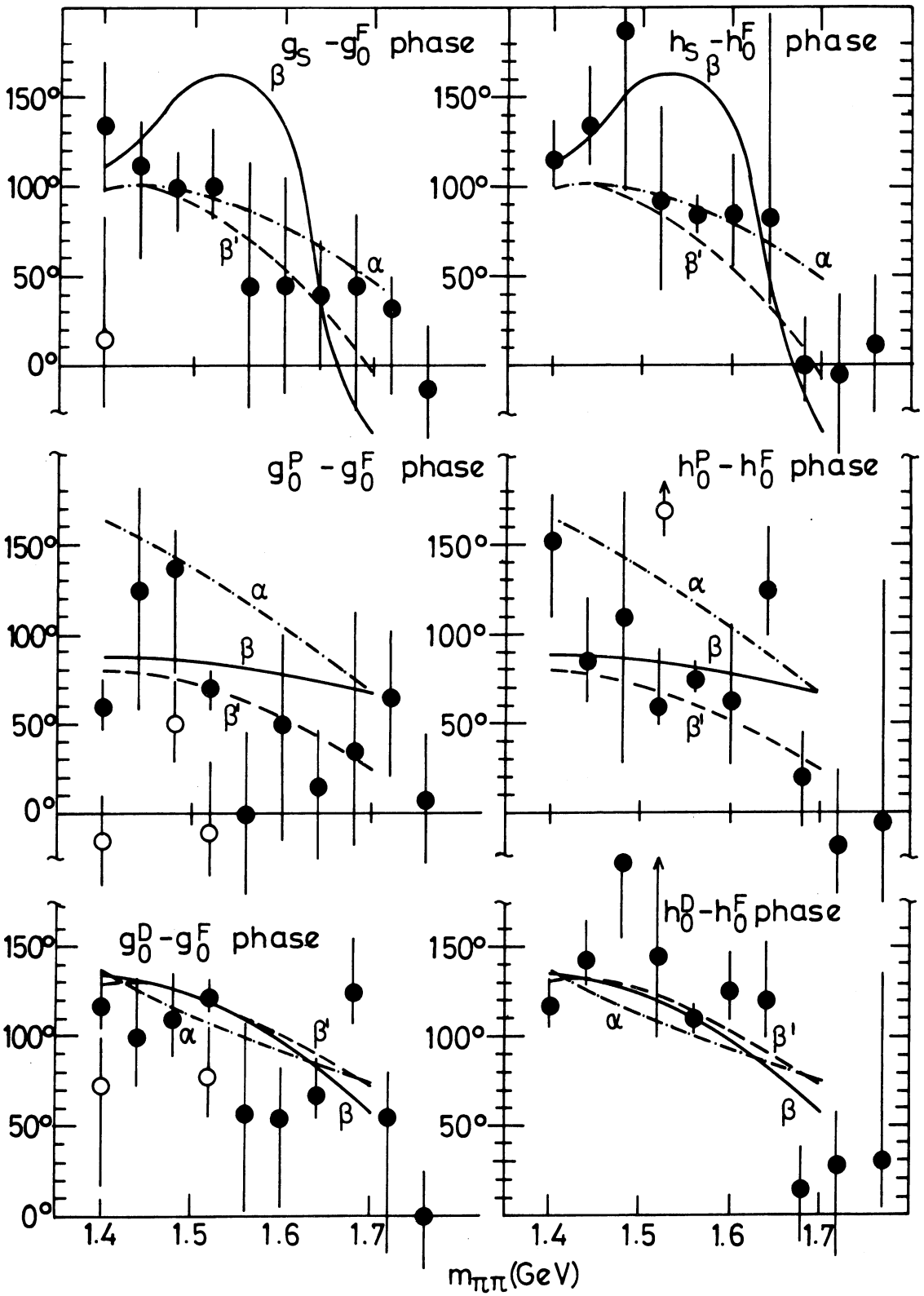
$g_S - g_0^F$ phase
$h_S - h_0^F$ phase
$g_0^P - g_0^F$ phase
$h_0^P - h_0^F$ phase
$g_0^D - g_0^F$ phase
$h_0^D - h_0^F$ phase
150°
100°
50°
0°
α
β
β'
1.4
1.5
1.6
1.7
$m_{\pi\pi}$(GeV)

Fig. 10

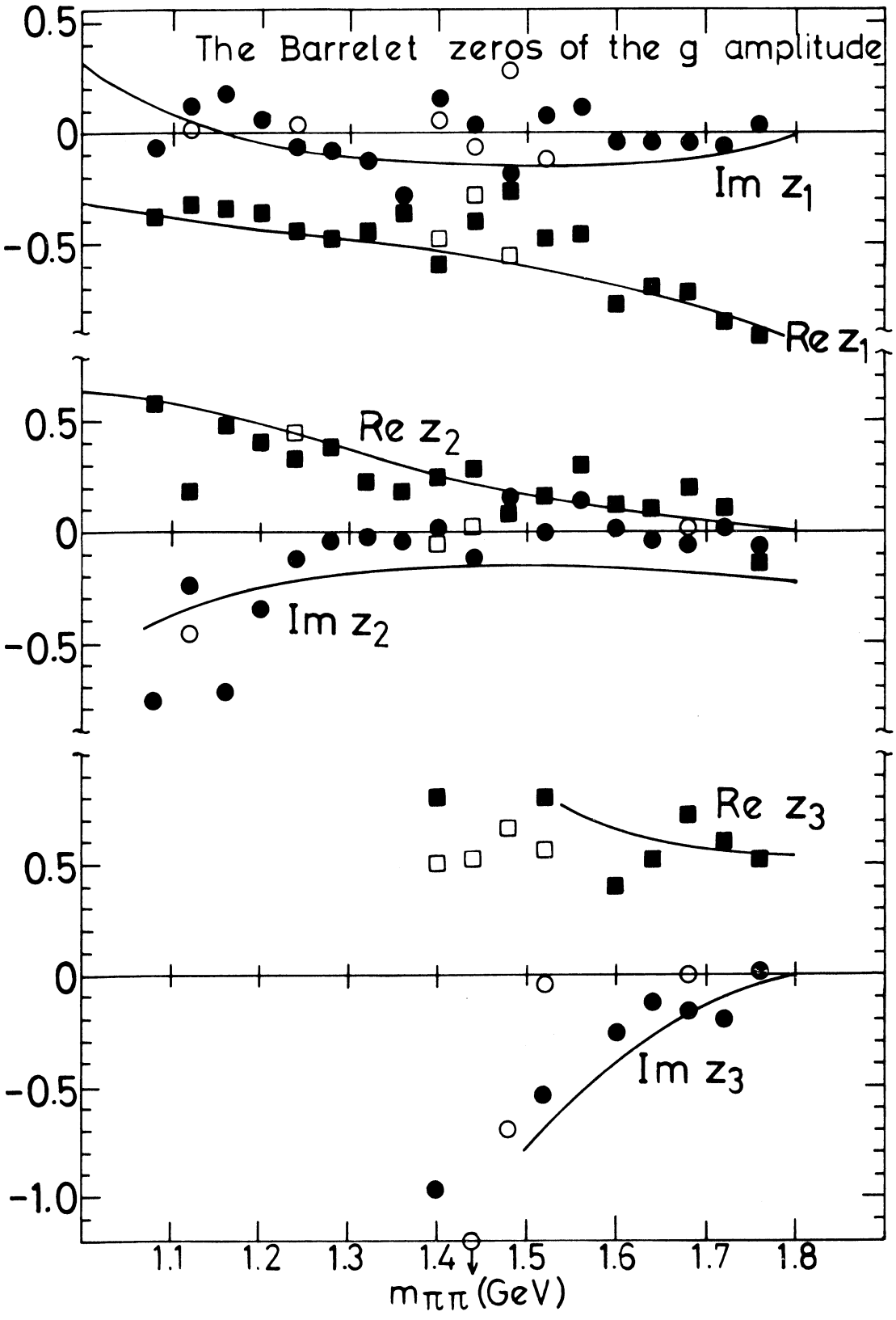
The Barrelet zeros of the g amplitude
Im z1
Re z1
Re z2
Im z2
Re z3
Im z3
0.5
0
-0.5
-1.0
1.1
1.2
1.3
1.4
1.5
1.6
1.7
1.8
mππ (GeV)

Fig. 11a

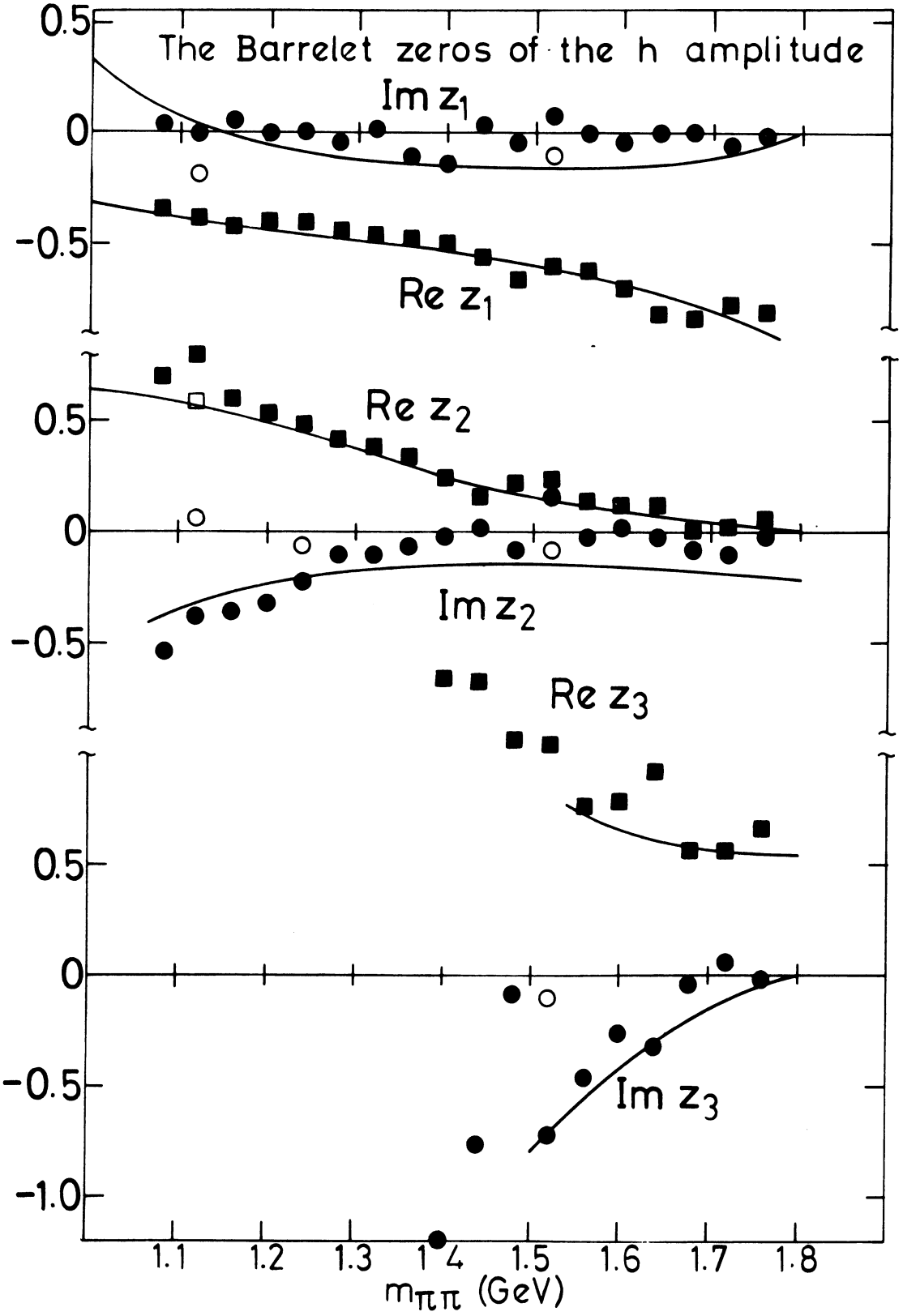
The Barrelet zeros of the h amplitude
Im z_1
Re z_1
Re z_2
Im z_2
Re z_3
Im z_3
0.5
0
-0.5
-1.0
1.1
1.2
1.3
1.4
1.5
1.6
1.7
1.8
$m_{\pi\pi}$ (GeV)

Fig. 11b